An enzyme for nucleotide sugar modification in *A. baumannii*

By Heather Clift

A thesis submitted in partial fulfilment of the requirements for the degree of

Masters of Research (MRES)

Department of Chemistry and Biomolecular Sciences

Macquarie University

15th of October, 2014

Contents

Acknowledgements

This past year has been one of the most memorable in my life, with all my newly gained knowledge and all of the people who contributed to it. I would like to start by thanking my supervisor A/Prof Bridget Mabbutt. She has been a great support throughout the entire process, sparking my interest in protein research and even molecular biology. She has also been paramount in teaching me how to write a proper thesis, and for this I will forever be grateful. Special thanks go to Bhumika who started this research, taught me everything I needed to know to get started, and stepped in to proofread at the end. I would also like to thank the other members of the Protein Structure Laboratory, Francesca and Jacob, who have helped me when I needed it and have been good company in the lab and office.

My thanks also go to Prof Ian Paulsen and Karl for teaching me all about molecular biology and letting me use their reagents and facilities. Thank you to Prof Nicki Packer for the donation of nucleotide sugars I needed and to Liisa for teaching me how to use the ITC.

Finally I would like to thank my parents and partner for their continual support in life, especially to my parents who helped me move across the world to go back to university. Without them I wouldn't be where I am today.

Abbreviations

Abbreviations are used in this work according to the format observed by the Journal of Molecular Biology (Elsevier). Special terms are used as follows:

ADH	alcohol dehydrogenase
CA-AB	community-acquired *A. baumannii*
DSF	differential scanning fluorimetry
EC	European clone
FucNAc	*N*-acetyl-L-fucosamine
GalNAc	*N*-Acetyl-D-galactosamine
GI	genomic island
GlcNAc	*N*-acetyl-D-glucosamine
IC	international clone
ICU	intensive care unit
IMAC	immobilised metal affinity chromatography
ITC	isothermal titration calorimetry
K_{av}	partition coefficient
LC	liquid chromatography
LSm	like SM
MDR	multidrug-resistant
NADP	nicotinamide adenine dinucleotide phosphate
PDB	Protein Data Bank
SDR	short-chain dehydrogenase/reductase
SEC	size exclusion chromatography
TCEP	*tris*(2-carboxyethyl)phosphine
T_m	melting temperature
UDP	uridine diphosphate
V_e	elution volume

Abstract

The Gram-negative bacillus *Acinetobacter baumannii* is an emerging multidrug-resistant, opportunistic pathogen responsible for severe nosocomial and community pneumonia outbreaks worldwide. Increasing resistance to antibiotics is thought to be due in part to highly variable genomic islands and lateral gene transfer. To date there have been studies into multiple genes in *A. baumannii* that are thought to play major roles in its resistance capabilities. One such gene found in a genomic island of the D1279779 strain of *A. baumannii*, *fnlA*, encodes for the protein *Ab*-WbjB, an extended short-chain dehydrogenase/reductase (SDR). Although it is similar in structure to other members of the SDR family, little is known about its function in *A. baumannii*.

I have carried out analysis on the active site chemistry of *Ab*-WbjB, discovering the necessity for the presence of its cofactor NADP for both overall protein stability and substrate binding. I have also found that *Ab*-WbjB binds to the substrate analogue UDP-GlcNAc. In addition to functional assays of the protein, an attempt at crystal growth was made under conditions containing both NADP and UDP-GlcNAc. A knockout of the *fnlA* gene in *A. baumannii* was also planned, but has yet to be completed.

Chapter 1: Introduction

1.1 Prevalence of *Acinetobacter baumannii* infections

The aerobic, Gram-negative bacteria *Acinetobacter baumannii* is an opportunistic pathogen seen mostly in immunocompromised individuals [1]. It has a high incidence in hospital environments, especially in intensive care units (ICUs) where patients are admitted for, on average, greater than 90 days [2]. Outbreaks have also been seen in war zones such as Iraq and in isolated communities in tropical Australia and Asia [3, 4] The prevalence of *A. baumannii* in ICUs is due to factors such as its multidrug-resistance (MDR), the ability to form biofilms on abiotic surfaces such as metals and plastics, and on occasion poor hygiene from hospital staff [5-7]. Due to these characteristics and the bacterium's preference for moist environments, pneumonia has become a problem in patients that have had breathing tubes inserted, as the bacteria bind to the surface of the tube and cause infection [1]. Beyond hospital settings, community-acquired *A. baumannii* (CA-AB) infections have also been reported in tropical regions such as Northern Australia and Asia [8]. CA-AB infected patients usually have in addition a severe underlying disease such as diabetes mellitus and chronic obstructive pulmonary disease, or a history of heavy smoking or excessive alcohol consumption. These reported cases are worrying as they have high mortality rates in the range from 40 to 64 % [4].

Epidemiological studies of nosocomial *A. baummannii* has revealed that there are three dominant clonal lineages spread around hospitals throughout the world, originally called European clones I, II, and III (ECI, ECII, and ECIII) [9]. ECI and II are broadly distributed and highly resistant to broad spectrum antibiotics. For instance, ECI strains are frequently resistant to expanded-spectrum cephalosporins, carbapenems, amikacin, and tigecycline [5, 10, 11].

Comparative genomic analyses of several strains of *A. baumannii* have revealed extraordinary plasticity of this bacterium [12]. This has been mainly attributed to the lateral gene transfer events [13]. Lateral gene transfer is known to occur through transmission of plasmids, transposons, phage, and integron gene cassettes between similar bacterial species [5]. These regions of shared genomic information are often clustered together in highly

variable genomic islands (GIs) [14, 15]. GIs are defined as a broad and diverse group of DNA elements which occur as discrete segments of laterally-acquired accessory sequences containing functionally-related genes with limited phylogenetic distribution [16]. These islands often include antibiotic resistance and virulence genes, symbiosis genes [17], sucrose and aromatic compound metabolism genes [18], and mercury resistance and siderophore synthesis genes [19]. They are thought to give GIs higher variability than mutations alone [15]. For example, the ECI strain *A. baumannii* AYE has an 86 kb GI, which contains 45 resistance genes conferring resistance to a broad range of antibiotics [20].

1.2 Discovery of WbjB in polysaccharide synthesis clusters

To date there have been studies into multiple genes and proteins in *A. baumannii* that are thought to play major roles in its virulence capabilities. A *csu* operon, along with an associated regulator region, was identified as being essential for pili formation [6, 21]. In addition, a few proteins have been found essential in biofilm formation, including Bap and OmpA, with further studies showing that OmpA also has a role in inducing apoptosis [22-24]. However, until recently, not much work has gone into identifying the function of novel genes in the genomic island regions of *A. baumannii*. Last year nine *A. baumannii* strains (see Table 1.1) and one *Acinetobacter baylyi* strain (ADP1, [25]) were compared in order to identify unique genomic regions (genomic islands (GIs)) for further investigation (Bhumika Shah, Sasha Tetu, Ian Paulsen and Bridget Mabbutt, unpublished data). After analysis, 87 GIs containing a combined 1632 genes were identified to be unique across all ten strains. These genes were then subjected to a protein structure pipeline approach at Macquarie University [26-28].

***Ab*-WbjB**, a protein from the *A. baumannii* community isolate D1279779, resulted from this pipeline approach. It acquired its name from a similar protein discovered in *Pseudomonas aeruginosa* (**WbjB** from *A. baumannii* will be referred to as ***Ab*-WbjB** throughout this thesis to avoid confusion with the enzyme found in *P. aeruginosa*). WbjB was found to be the first of three enzymes in a pathway that changes the structure of nucleotide sugars [29]. The other two enzymes in this pathway are WbjC and WbjD respectively. The proposed series of reactions performed by these enzymes turn one nucleotide sugar,

Table 1.1. *A. baumannii* strains compared in previous work [16].

clonal lineage	strain	origin	reference
ECI group	BALI155	Australia	unpublished
	AB307 0294	U.S.A	[30]
	AB0057	U.S.A	unpublished
	AYE	France	[31]
ECII group	WM99c	Australia	unpublished
	ACICU	Italy	[32]
Non-EC group	D1279779	Australia	[12]
	ATCC 17978	France	[33]
	SDF	France	[31]

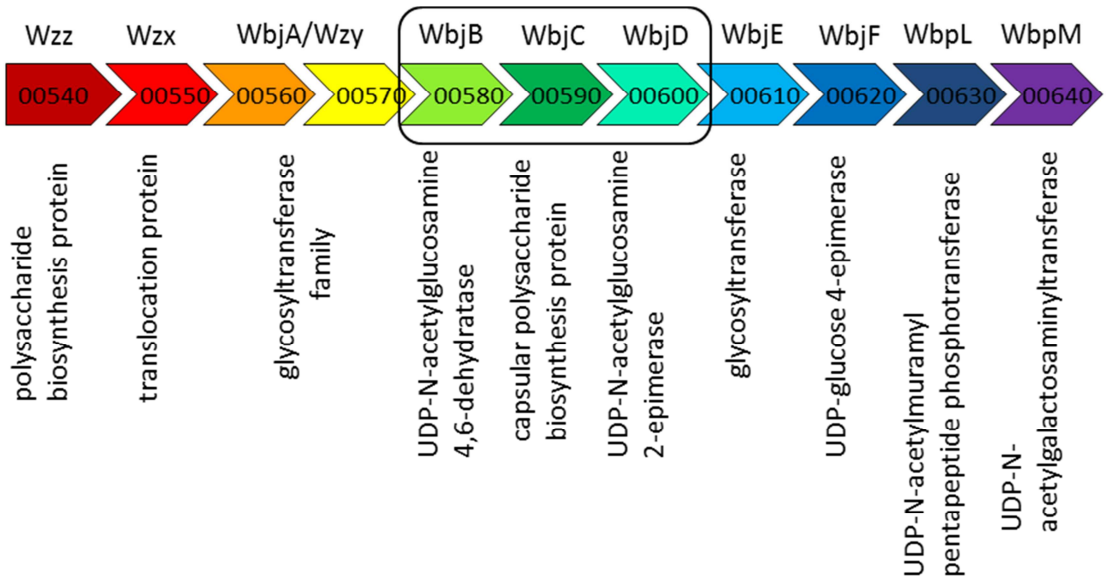

Fig. 1.1. Polysaccharide synthesis cluster found in both *A. baumannii* D1279779_RGP01 and *P. aeruginosa* O11. The numbers in the arrows are the gene ID numbers from D1279779 with the predicted protein function listed below. Above the arrows is the synonymous protein name found in *P. aeruginosa*. The WbjBCD group of proteins has been boxed.

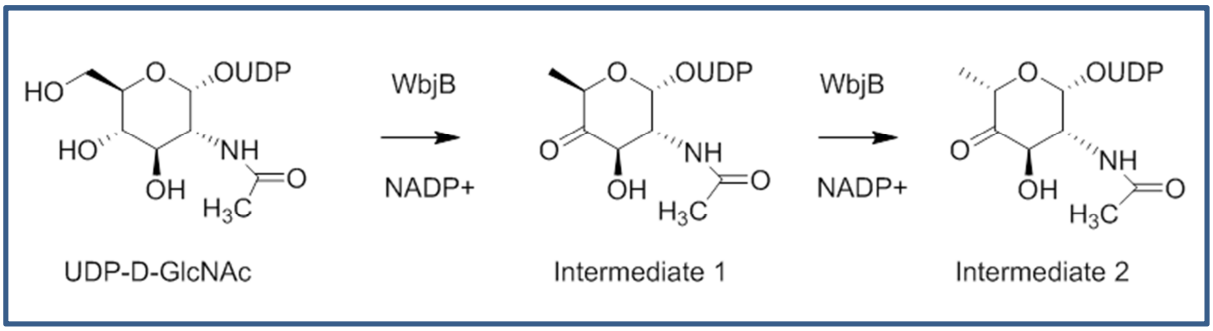

Fig. 1.2. Reaction performed by WbjB. Substrate dehydration followed by epimerization performed by WbjB starting with UDP-D-GlcNAc. Intermediate 1 is UDP-2-acetamido-2,6-dideoxy-α-D-xylo-4-hexulose and Intermediate 2 is UDP-2-acetamido-2,6-dideoxy-β-L-arabino-4-hexulose [29].

UDP-*N*-acetyl-D-glucosamine (UDP-GlcNAc), into UDP-*N*-acetyl-L-fucosamine (UDP-L-FucNAc). The part of the genome that WbjB was found to occupy in *P. aeruginosa* shows sequence similarity to the area of the GI studied in *A. baumannii*. Fig. 1.1 shows the full polysaccharide synthesis cluster in which the gene encoding WbjB is found. It is comprised of eleven genes, arranged in the same order both in *A. baumannii* and *P. aeruginosa*. Between the two WbjB genes there is an 81% sequence identity [16].

In *P. aeruginosa*, WbjB is bifunctional and is thought to perform the first two steps in the enzymatic pathway described above. The first is the C-4, C-6 dehydration of UDP-GlcNAc, resulting in the first of two intermediates seen in Fig. 1.2. The second step involves a C-5 epimerization, resulting in Intermediate 2. From this sugar WbjC and WbjD continue the pathway, leading to the synthesis of UDP-FucNAc [29]. This sugar product is thought to make up the repeating units of sugars found in LPS O antigens of *P. aeruginosa* [29].

O antigens are attached to the lipid A core of LPS and are found in Gram-negative bacteria covering the surface of the outer membrane. Even though *A. baumannii* is a Gram-negative bacterium it has been speculated that it displays no O antigens, and that the sugars produced by the ***Ab*-WbjBCD** enzymes make up K antigens [34]. K antigens are located on the outside of the capsule in Gram-positive and Gram-negative bacteria and are essential in the processes of cell recognition and defence [35].

Surface sugars, or glycans, are an important part of a cell's defences against attack from host immune systems. These sugars present a method by which bacteria can continually disguise themselves against attack [36]. Gram-negative bacteria have lipopolysaccharides (LPS) on the outside of their cells and have formed mechanisms to modify these structures after initial synthesis [37]. The lipid A core and the attached groups can undergo extensive remodelling which allows bacteria to increase resistance to antimicrobial peptides and interfere with the host's ability to recognise LPS as a conserved microorganism-associated molecular pattern [38]. As pathways like the one described above are absent in humans, the surface glycans of bacteria are a possible target when devising vaccines or medications against infection. Using fragments of LPS has been a method for vaccination for many decades [39].

1.3 Short-chain dehydrogenase/reductase enzyme class

Short-chain dehydrogenases/reductases (SDR) constitute a large family with about 2000 forms known [40], including species variants. SDRs are simple, one-domain NAD(P)(H)-dependent enzymes that usually have a length of about 250 amino acid residues (extended SDRs have an additional 100 residues) [40].

The SDR gene family is highly divergent, with typically 15%–30% residue identity in pairwise comparisons. In spite of the low residue identities between the different members, the folding pattern is conserved with largely superimposable peptide backbones [41-43]. They also have several highly conserved binding motifs, with 24-46% of residues strictly conserved [43]. In these enzymes the cofactor-binding site is a Gly-rich area that includes a basic residue and takes the form of a Rossmann fold (Fig. 1.3, A) composed of a central, twisted parallel β-sheet consisting of approximately 6-7 strands which are flanked by 3-4 α-helices from each side [44].

SDRs have been functionally linked to a host of metabolic functions encompassing mostly dehydrogenases/ reductases, lyases or isomerases [43]. The substrate-binding site of SDRs (Fig. 1.3 and 1.4) shows more variation than the cofactor-binding site, but generally consists of a canonical catalytic triad, Ser/Thr with a TxxxK motif, found at the C-terminal end [40, 45]. The substrates for SDRs range from alcohols and sugars, to steroids, xenobiotics, and aromatic compounds. The recurrence of SDR enzymes within bacteria such as *A. baumannii*

[16] signifies that this functional diversity may confer ideal adaptive GI componentry for pathogenic organisms.

1.4 Structural insights of *Ab*-WbjB

The crystal structure of ***Ab*-WbjB** was solved to 2.65 Å at the Protein Structure Laboratory, Macquarie University. The three-dimensional structure of ***Ab*-WbjB** is illustrated in Fig. 1.3. It reveals three well-defined regions for each protomer. The largest domain contains a nine-stranded β-sheet, flanked on either side by seven α-helices. This formation is based on the characteristic Rossmann fold known to serve as the nucleotide-binding region in all SDRs [46]. The smaller C-terminal region of ***Ab*-WbjB** is essentially composed of four α-helices and two small β-strand segments, one parallel set and one anti-parallel. This C-terminal region and its interconnecting linking segments display a flexible conformation and are likely to be involved in substrate binding. Very high B factors, as depicted in Fig. 1.3, B, are observed in these regions reflecting their dynamic mobility. This region also interfaces additional protomers of the hexamer [16].

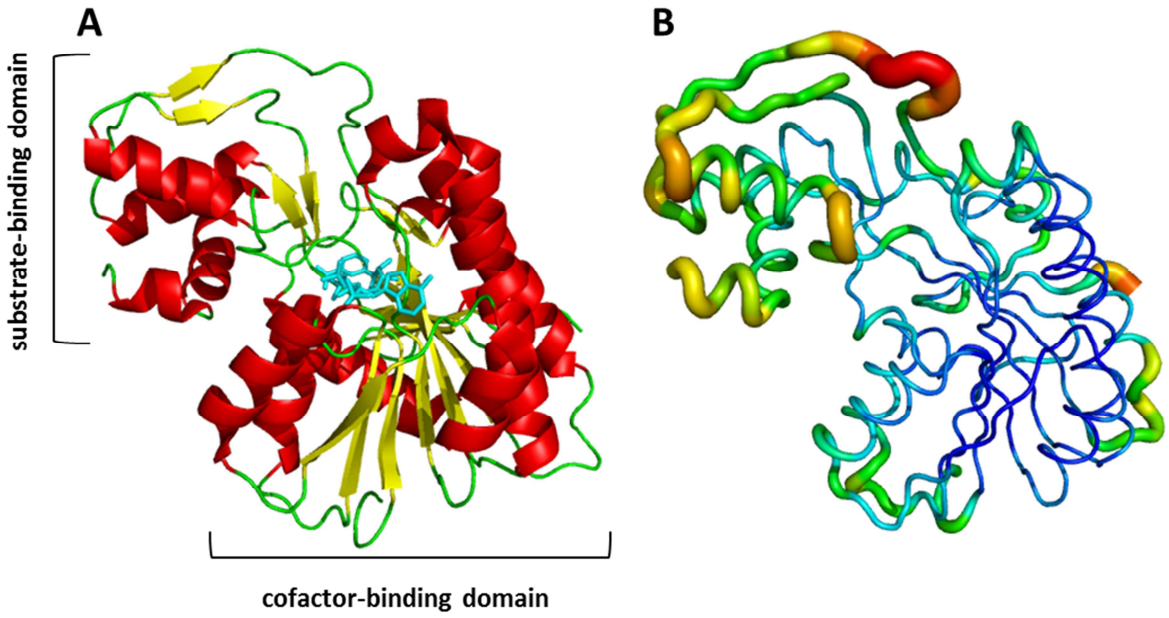

Fig. 1.3. Crystal structure of ***Ab*-WbjB**. (A) ***Ab*-WbjB** displaying secondary structure elements (red: helix, yellow: β-sheet, green: loop). NADP bound within the Rossmann fold can be seen in this structure. (B) The ***Ab*-WbjB** structure in cartoon representation in B-factor putty mode to reflect the thermal flexibility of the structure (red: high B-factor to blue: low B-factor).

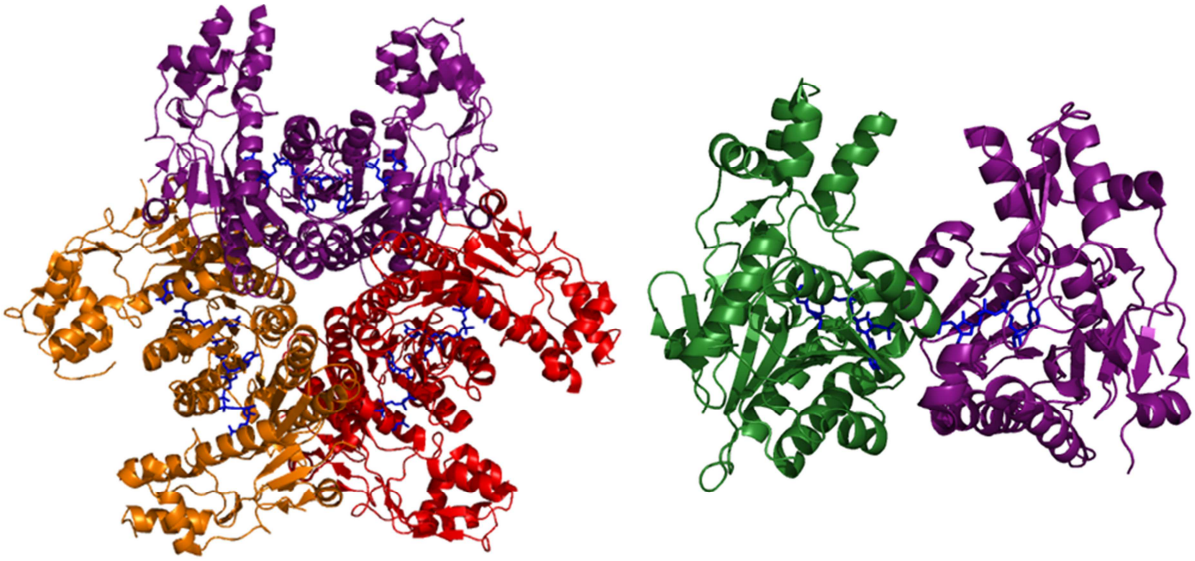

Fig. 1.4. On the left is the hexameric form of ***Ab*-WbjB** with each dimer coloured differently. Also shown is NADP in blue. To the right is the dimeric form of the enzyme (chain A and D) with each monomer coloured differently. NADP can still be seen in blue.

The crystal structure of ***Ab*-WbjB** reveals a hexameric protein, displaying a trimer of dimers (Fig. 1.4). In spite of no NADP added either in the growth conditions or crystallisation cocktails, it was found in all six chains of the structure, as can be seen in the image above. This indicates that NADP interaction is strongly favoured by the enzyme. No bound substrate was observed in the structure of ***Ab*-WbjB**.

1.5 Structural homologs of *Ab*-WbjB

A search for structural homologs, performed using the PDB with the DALI server [47], to locate ***Ab*-WbjB**'s closest fold relatives revealed two very similar proteins. CapE, a capsular polysaccharide-synthesising enzyme from *Staphylococcus aureus*, has a sequence identity of 68% to ***Ab*-WbjB**, and the two are thought to bind the same cofactor and similar substrates [48]. FlaA1, a flagellar glycosylation protein found in *Helicobacter pylori* has 39% sequence identity with ***Ab*-WbjB**, but was crystallised and characterised much earlier than CapE, in 2006 [49].

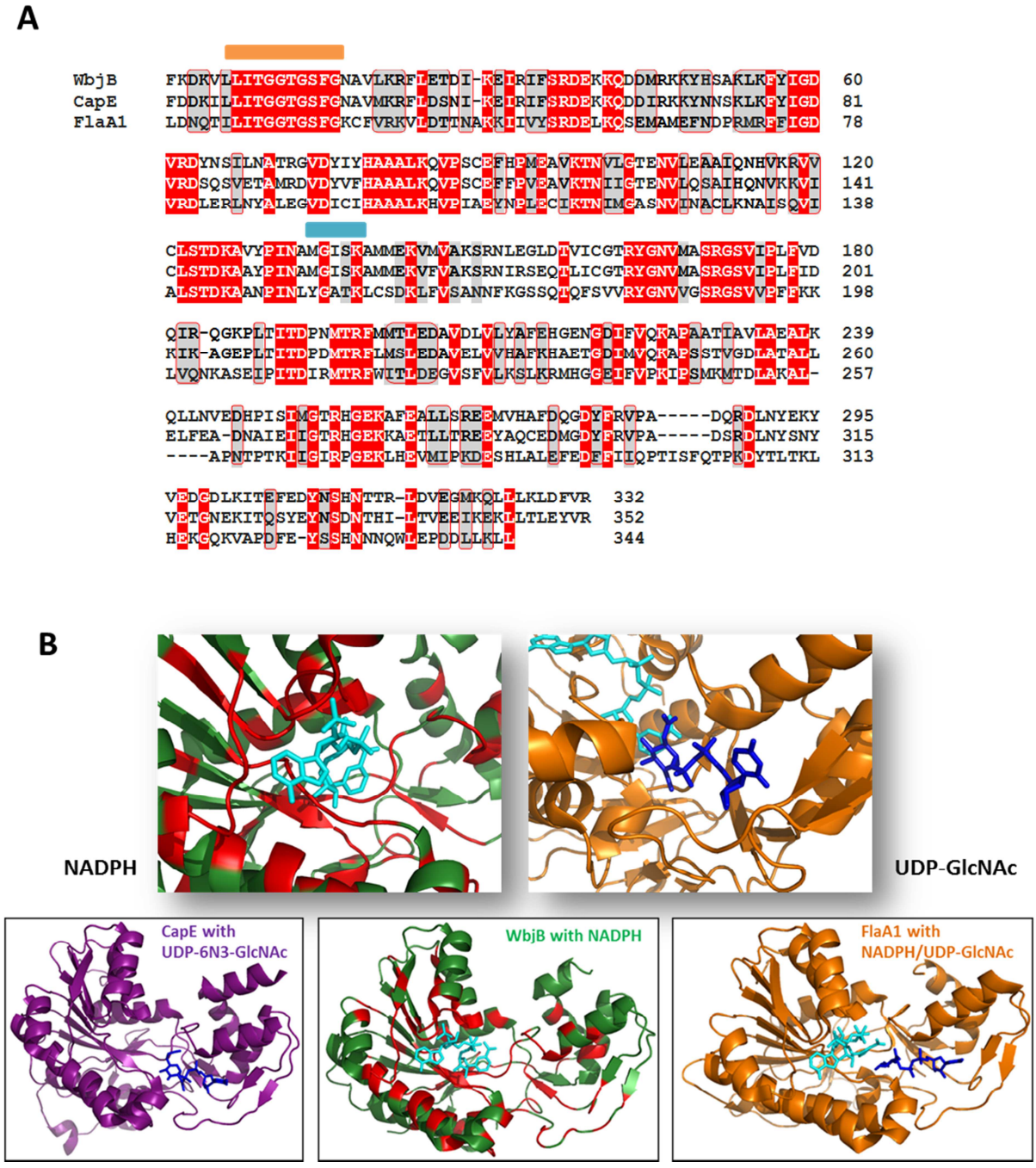

Fig. 1.5. Sequence alignment of structural homologs ***Ab*-WbjB**, CapE, and FlaA1. (A) Sequence alignment between ***Ab*-WbjB** (PDB 4j2o), CapE (PDB 3vvb), and FlaA1 (PDB 2gn4). The NADPH binding site (below the orange box) is highly conserved across each sequence, whereas the predicted substrate-binding site (below blue box) is less conserved. (B) Ribbon representation of each enzyme with cofactor and substrate seen when crystallised. The centre picture shows the fully conserved residue areas between all three proteins projected on ***Ab*-WbjB**.

CapE is the first enzyme in a pathway almost identical to that of WbjBCD which consists of CapEFG and produces UDP-FucNAc. The crystal structure of CapE published in 2013 (PDB 3w1v), shows that it forms a hexamer in solution, or a trimer of dimers, which is only seen in two other SDRs, one being ***Ab*-WbjB** and the other FlaA1 [16, 50]. As seen in ***Ab*-WbjB**, CapE displays the canonical catalytic triad (located beneath the blue box in Fig. 1.5, A) composed of a Met instead of the Tyr seen in most other SDRs (MxxxK, see section 1.3) [51]. Given the relatively high resolution of the CapE crystal structure (2.1 Å), a highly dynamic region near the substrate-binding pocket, named the latch, was discovered [48]. The latch is thought to regulate the access of substrate to the binding pocket as it is positioned at the entrance to this pocket. It was also speculated that the difference in residues found in the binding pocket (Met instead of Tyr) is tied to this novel latch structure [48]. Examination of CapE crystal structures with and without the inhibitor UDP-6N_3-GlcNAc (Fig. 1.5, B) shows presence of NADPH only in the unbound form [48, 51]. This is unusual as NADPH shows very high binding affinity for CapE. It is thus speculated that NADPH is released once the necessary dehydration and epimerisation of UDP-GlcNAc have occurred, similar to mechanisms displayed by SDR proteins ArnA and UDP-xylose [52]. It is also possible that the inhibitor is bound in a way that was not compatible with the concurrent binding of the cofactor [48].

A second structural homolog, FlaA1, is also a hexameric protein. It binds NADPH as a cofactor and is thought to bind UDP-GlcNAc as a substrate. However, unlike ***Ab*-WbjB** and CapE, FlaA1 is crystallised with both cofactor and substrate bound (PDB 2gn4, Fig. 1.5, B) [50]. FlaA1 is thought to play a role in glycosylation of flagella as well as the synthesis of the O antigen section of LPS [53, 54].

Sequence alignment of these proteins can be seen in Fig. 1.5, A. It is shown that the cofactor-binding site in all three enzymes is fully conserved, consisting of the Gly-rich region previously described, but the substrate-binding site is more varied. The active site motif is conserved between ***Ab*-WbjB** and CapE, but not FlaA1. FlaA1 displays the YxxxK motif, whereas ***Ab*-WbjB** and CapE contain the less utilised MxxxK motif. Fig. 1.5, B compares the crystal structures of homologs, with either cofactor, substrate, or both bound.

1.6 Aims of my work

The increasing prevalence of *A. baumannii* related infections is emerging as a serious health care problem. ***Ab*-WbjB**, an SDR enzyme encoded by a GI in *A. baumannii* community isolate D1279779, has been identified to play an important role in polysaccharide biosynthesis, likely contributing to *A. baumannii*'s virulence mechanism. It is therefore important to understand the precise role of this enzyme so as to gain insights into what makes *A. baumannii* unique as well as understand its capacity for adaptation.

My study focuses on functionally characterising the substrate-binding site of ***Ab*-WbjB** to determine the role of ***Ab*-WbjB** within *A. baumannii*. Therefore, the specific aims of my project were to:

I) Measure relative protein stability through fluorescence binding assays in the presence of probable substrate analogues;
II) Detect specific binding events of suspected substrate utilising calorimetric assays;
III) Probe active site chemistry by using site-directed mutagenesis of key residues;
IV) Interrogate substrate-binding mechanisms by co-crystallising ***Ab*-WbjB** in the presence of a substrate analogue;
V) Investigate phenotypic differences by generating an *fnlA* gene knockout in *A. baumannii*.

Chapter 2: Materials and Methods

2.1 Reagents

All chemical reagents used were of analytical grade or higher and were generally obtained through mainstream suppliers (Astral, Gymea NSW 2227 Australia, VWR International, and Sigma-Aldrich). For cloning and gene expression, 1XLBlue cells (Agilent) and BL21(DE3) pLysS cells (Novagen) were used. Primers were ordered through Integrated DNA Technologies (Baulkham Hills, NSW) and DNA sequencing was processed by Macrogen (Seoul, Republic of Korea). Kits for DNA extraction (QIAprep Spin Miniprep), purification (QIAquick PCR Purification) and gel extraction (QIAquick Gel Extraction) were supplied by QIAGEN. Purified water from a MilliQ system (Millipore) was used for preparation of all buffers and reagents.

Table 2.1. Composition of growth media

Growth Media/Buffer (1 L)	Composition	Reference
SOC medium	20 g tryptone, 5 g yeast extract, 0.58 g NaCl, 0.18 g KCl, 0.95 g $MgCl_2$, 1.20 g $MgSO_4$, 20 % glucose (added after autoclaving)	[57]
Lysogeny Broth (LB)	10 g tryptone, 5 g yeast extract, 10 g NaCl	[58]
5052 media (50x)	250 g glycerol, 25 g glucose, 100 g α-lactose	[59]
NPS media (20x)	66 g $(NH_4)_2SO_4$, 136 g KH_2PO_4, 142 g Na_2HPO_4 (pH 6.75)	[59]
ZY media	10 g tryptone, 5 g yeast extract	[59]
ZYP-rich media	1 ml 1 M $MgSO_4$, 20 ml 50x 5052 media, 50 ml 20x NPS, 1 L ZY media	[59]
LB agar	10 g tryptone, 5 g yeast extract, 10 g NaCl, 15 g bacteriological agar	[57]
M9 salts	15 g KH_2PO_4, 64 g $Na_2HPO_4 \cdot 7H_2O$, 2.5 g NaCl, 5 g NH_4Cl	[57]

Table 2.2. Components used for PCR

Components[1]	Colony PCR	Infusion cloning PCR
sterile water	31.8 µl	38.6 µl
commercial buffer	10 x Taq buffer (5 µl)	10 x Pfu buffer (5 µl)
dNTPs (10 mM)	1 µl	1 µl
forward primer	(gene-specific *fnlA*) 1 µl	125 ng
reverse primer	(plasmid-specific T7) 1 µl	125 ng
target DNA	10 µl	100 ng
DNA polymerase	Taq (0.2 µl)	Pfu Turbo (1 µl)

[1] *All reagents provided by QIAGEN (Taq Polymerase Kit), with exception of Pfu buffer (Invitrogen) and Pfu Turbo polymerase (Agilent).*

Strains of *Escherichia coli* were cultured in/on Luria Bertani (LB) medium (Table 2.1) at 37 °C, unless otherwise stated. Aside from recovery steps during transformation, cells were grown in/on medium containing appropriate concentrations of antibiotics (25 µg/ml chloramphenicol or tetracycline, 50 µg/ml ampicillin) to select for or maintain incorporated plasmids. All microbiology methods were conducted in sterile conditions, maintained by flame. All media and buffers are described in Table 2.1, and all media preparations (1 L) were autoclaved before use.

2.2 Molecular biology procedures

2.2.1 Establishment of competent cell stocks

Previously, the gene *fnlA* from *Acinetobacter baumannii* D127997 [12] was cloned into a pET15b vector and then transformed into competent BL21 (DE3) pLysS *Escherichia coli* cells by Dr. Bhumika Shah (Macquarie University) and stored as glycerol stocks (HC_***Ab*-WbjB** pLysS) [16, 55, 56]. These cells are the source of expression for the protein (***Ab*-WbjB**) required for my project. In order to confirm that this gene insert was still present in pET15b, HC_***Ab*-WbjB** pLysS cells were grown overnight in LB (5 ml with ampicillin). The DNA was extracted and sent with both T7 primer (vector-specific) and gene-specific primer for sequencing. Colony PCR (Table 2.2) was subsequently carried out on the vector in a 50 µl mix using the following thermal cycle (94 ˚C for 3 min, 30 rounds of 94 ˚C for 30 s, 55 ˚C for 30 s, and 72 ˚C for 30 s, and final extension at 72 ˚C for 5 min).

For electrophoresis, a 1.2 % (w/v) agarose gel was made in 50 ml 1 x TAE buffer (80 mM Tris buffer, 0.7 % (v/v) acetic acid, with pH 8.0 2 mM EDTA). Following the addition of 1 µl commercial dye (GelRed, Biotium), samples were run in 1 x TAE buffer at 100 V for 90 min. Bands were visualized under UV light.

2.2.2 Site directed mutagenesis

To prepare mutations in gene product ***Ab*-WbjB**, primers were designed within OligoCalc [60] to have a melting temperature of 78 ˚C and a GC content close to 40 % (Table 2.3). Primers were diluted (1:10) to make a working stock (20 µl). Infusion cloning PCR was then performed on the pET15b plasmid with *fnlA* gene insert (reagents of Table 2.2) according to the previously described temperature cycle (section 2.1.2.1). To each PCR product Dnp1

Table 2.3. Primers used to create site specific mutants of ***Ab*-WbjB**

Gene product	Primer sequence (5' - 3')
C89A	F – CAGGTACCATCTGCGGAGTTTCACCCAATGGAAGCTG
	R - CAGCTTCCATTGGGTGAAACTCCGCAGATGGTACCTG
S123A	F – CCATGTTAAACGTGTAGTGTGTTTAGCGACTGATAAAGCAGTTTACCC
	R - GGGTAAACTGCTTTATCAGTCGCTAAACACACTACACGTTTAACATGG
M134A	F – GCAGTTTACCCAATTAATGCAGCGGGTATTTCTAAAGCCATGATGG
	R - CCATCATGGCTTTAGAAATACCCGCTGCATTAATTGGGTAAACTGC
M134L	F – GCAGTTTACCCAATTAATGCACTCGGTATTTCTAAAGCCATGATGG
	R – CCATCATGGCTTTAGAAATACCGAGTGCATTAATTGGGTAAACTGC
M134Y	F – GCAGTTTACCCAATTAATGCATACGGTATTTCTAAAGCCATGATGG
	R – CCATCATGGCTTTAGAAATACCGTATGCATTAATTGGGTAAACTGC
Y164F	F – CGGTTATTTGTGGCACTCGTTTCGGTAATGTGATGGCATCACG
	R - CGTGATGCCATCACATTACCGAAACGAGTGCCACAAATAACCG

enzyme was added (1 µl, Agilent) and left to incubate (37 ˚C, 1 h). Transformation of Dnp-treated DNA (1.5 µl) into thawed competent 1XLBlue cells (50 µl) was started by incubation on ice (30 min). Samples were heat shocked (30 s, 42 ˚C) and put back on ice (2 min). SOC medium (500 µl at room temperature) was added to samples and left to incubate (2 h) with shaking (37 ˚C, 250 rpm). High and low volume samples (150 µl and 350 µl) were plated onto LB agar with ampicillin resistance to select for positive clones. Colonies were picked and replated. Tips used for picking colonies were added to LB (10 ml with ampicillin) and medium grown up for two days (25 ˚C, 250 rpm).

Plasmid extraction was performed and the purified DNA sequenced. For creation of stock, cultures (5 ml) were spun down (10 min, 2200 *g*) and recovered cell pellets resuspended in M9 salts (750 µl) and glycerol (50 %, 750 µl). Glycerol stocks for each of the six strains (HC_1XLB_C89A, HC_1XLB_S123A, HC_1XLB_M134A, HC_1XLB_M134L, HC_1XLB_M134Y, and HC_1XLB_Y164F) were stored at -80 ˚C.

Transformation of extracted plasmid into BL21(DE3) pLysS cells was carried out as stated previously. Cultures were plated in high and low volume (100 µl and 300 µl) onto LB agar

with ampicillin and chloramphenicol selection. Colonies were chosen and restreaked onto fresh plates. Glycerol stocks were then made of this cell line as above (HC_DE3_C89A, HC_DE3_S123A, HC_DE3_M134A, HC_DE3_M134L, HC_DE3_M134Y, HC_DE3_Y164F).

2.2.3. Gene knockout construction

In order to knockout *fnlA* in *A. baumannii* D1279779 [12], primers were designed with the help of Primer 3 [61] for a melting temperature of 70 ˚C and a target GC content of 50 % (Table 2.4).

PCR was carried out (Table 2.2) with substitution of *Taq* buffer (0.4 µl) and *Taq* polymerase for Pfu components, and the addition of $MgCl_2$ (25 mM, 2 µl). A combination of primers and template DNA was used in order to prepare three distinct PCR constructs. Up primers (0.8 µM) and their matching Dn primers (0.8 µM) were combined with D1279779 DNA (50 ng) to form two constructs. Primers Up_R and Dn_F (0.2 µM) were combined with Kanamycin (Km) DNA (14.5 ng) to form the third construct (PCR cycles according to previously published method [24]). PCR products were purified and checked for purity by agarose gel electrophoresis.

The three constructs were then combined in a second-round PCR reaction (5 µl 10x KOD buffer, 3 µl 25 mM $MgCl_2$, 5 µl 2 mM dNTPs, 1 µl KOD Hotstart polymerase (Biolabs), 30 µl water) using the following thermal cycle (95 ˚C for 2 min, five rounds of 95 ˚C for 20 s, 65 ˚C

Table 2.4. Primer sequences for manipulation of *fnlA* in *A. baumannii*

Primer name	Sequence (5’ - 3’)
Up_F fnlA	GCCGCGAGGATCCCAACAGCAATGCCAAGAAAC
Up_R fnlA	ATTACGCTGACTTGACGGGACCAAATGATCCTGTACCACCA
Dn_F fnlA	GAGCTGCCAGGAAACAGCTACGCATTAACAAGAGGCGAAT
Dn_R fnlA	GGCCGGCCTGCAAAAATTTCATTCGCCCACAG

for 15 s, and 72 ˚C for 90 s). This cycle was then paused to add Up_F and Dn_R primers (1 µl each) and continued as follows (30 rounds of 95 ˚C for 20 s, 65 ˚C for 15 s, and 72 ˚C for 90 s, and final extension at 72 ˚C for 1 min). Products were again checked by electrophoresis.

An *E. coli* cell line (DH10B) (courtesy Ian Paulsen, Macquarie University) provided a source for the plasmid pEX18Tc, required for uptake of the complete construct. DH10B cells were grown up in LB containing tetracycline. Cells from this culture were used for plasmid extraction and creation of a glycerol stock.

The complete construct and plasmid pEX18Tc were digested with restriction enzymes BamHI (1 µl for 2 h, Promega) and PstI (1 µl for 2 h, Biolabs) in two separate 30 µl reactions (20 µl DNA, 33 µg BSA, 3 µl 10x buffer 4, 37 ˚C). Reaction products were visualised by agarose gel electrophoresis and the digested DNA purified using gel electrophoresis and commercial PCR purification columns.

2.3 Protein expression

HC_***Ab*-WbjB** pLysS cells were grown in starter cultures of LB (5 ml with chloramphenicol and ampicillin). Cultures (5 ml) were poured into 2 L baffled flasks containing ZYP-rich media (500 ml), ampicillin and chloramphenicol and grown at 25 ˚C to OD_{600} of 1.2 – 1.3 for 24 h.

Cells were pelleted by centrifugation (5,000 *g*, 30 min) and resuspended in 25 ml of Buffer A (20 mM HEPES buffer (pH 8.0), 200 mM NaCl) containing protease inhibitor cocktail (275 µl) and glycerol (5 % (v/v)). Cells were disrupted by a freeze-thaw cycle, and then lysozyme (275 µl, 1mg/ml) and DNase I (20 µl, 5 mg/ml) were added to each aliquot. Lysis was achieved through sonication (S-2500 Branson Digital Sonifier, amps 60 %, 10 s on, 10 s off for 60 s). After centrifugation (11,000 *g*, 40 min), the released supernatant was filtered (0.2 µm syringe filter) on ice and filtrate was collected in 30 ml aliquots for purification.

2.4 Protein purification

All buffers and water were degassed and filtered before use in chromatography steps. Prepacked Ni-Sepharose immobilised metal affinity chromatography (IMAC) columns (His trap, GE-Healthcare) equilibrated first with water (10 cv) and subsequently with Buffer A (10 cv) before loading each under pressure with filtered cell lysate (30 ml) using a bench-top pump (Gibson mini-plus3). The IMAC columns were overloaded with protein and washed

with Buffer A with 50 mM imidazole (45 – 50 cv) to remove unbound extraneous proteins. His-tagged ***Ab*-WbjB** was eluted from IMAC columns at 0.5 ml/min on an LC system (Äkta Explorer, GE-Healthcare) using Buffer A with 500 mM imidazole. Fractions with A_{280} readings indicating protein at a concentration of 10 – 15 mg/ml were pooled, EDTA added to 1 mM, and each sample was dialysed into Buffer T (Buffer A with 0.5 mM *tris*(2-carboxyethyl)phosphine (TCEP)). Final protein samples were frozen for storage (-80 ˚C).

2.5 Protein analysis

2.5.1 Size exclusion chromatography

For analysis of ***Ab*-WbjB** samples in solution, a Superdex 200 10/300 GL matrix (GE-Healthcare) was utilised for size exclusion chromatography (SEC). The Superdex column was equilibrated with Buffer A with 5 % glycerol for 1 h on an LC system until pressure and conductivity had stabilized. Calibration was carried out with combinations of the following commercial standards: ferritin (440 kDa), aldolase (158 kDa), ovalbumin (43 kDa), RNase I (13.7 kDa), conalbumin (75 kDa), and carbonic anhydrase (26 kDa) (HMW and LMW calibration sets, GE-Healthcare). The void volume of the column was determined to be 8.5 ml using Blue dextran dye (GE-Healthcare). Elution volumes (V_e) of eluting proteins were converted to partition coefficient (K_{av}) values for this 24.0 ml column using the equation: $K_{av} = V_E – 8.5 / 24 – 13.5$. The linear relationship of K_{av} and log MW is shown in Fig. 2.1 and can be used to calculate the column performance ($R^2 = 0.9954$) to estimate the native mass of ***Ab*-WbjB** samples [62].

2.5.2. Protein electrophoresis

Purified proteins were visualised using SDS-PAGE (15 % separating and 5 % stacking gel) with a commercial protein ladder (Benchmark, Invitrogen) allowing estimation of protein size. Reagents used are itemised in Table 2.5. Samples (3 µl) were boiled in 2x loading dye (8 µl) for 15 min prior to loading. Electrophoresis was carried out at 100 V (10 min) and then at 120 V (1 h) in a Tris/glycine based buffer (see Running Buffer, Table 2.5). Gels were fixed for 10 min (Fixing Solution), stained for 5 min (Staining Solution), then destained for 2 h (Destaining Solution).

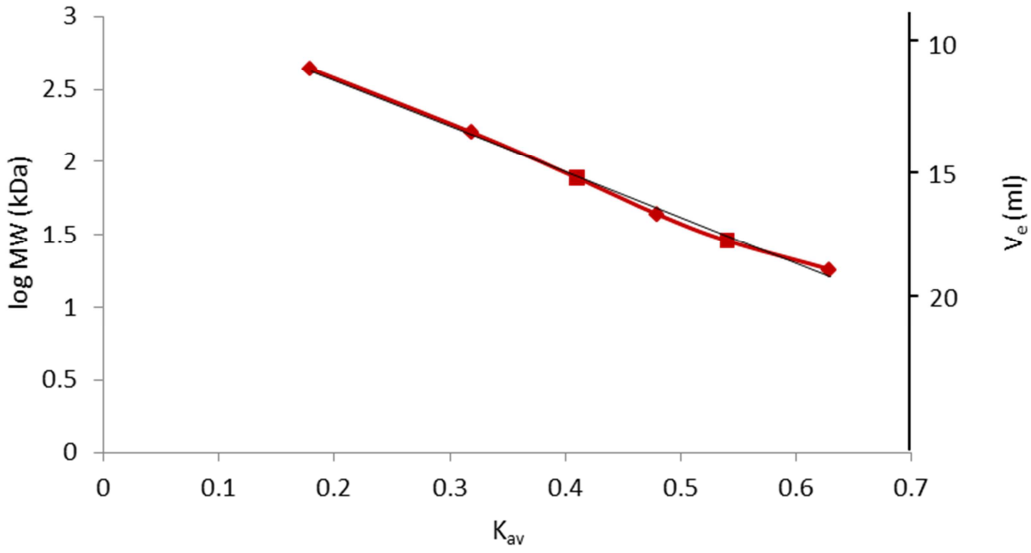

Fig 2.1. Performance of Superdex 200 10/300 GL matrix eluting with HEPES buffer (20 mM, pH 8.0) with 200 mM NaCl at flow rate of 0.5 ml/min. K_{av} values for commercial molecular weights standards are graphed. Linear regression yielded y = -3.1516x + 3.193 as best fit. V_0 of 8.5 ml was determined using Blue Dextran dye.

Table 2.5. Buffers and solutions for SDS-PAGE protein analysis

Buffer/solution	Composition
2 x loading dye	4 % (w/v) SDS, 20 % (v/v) glycerol, 200 mM DTT, 100 mM Tris buffer (pH 6.8), 0.2 % (w/v) bromophenol blue
Running Buffer	25 mM Tris buffer, 250 mM glycine, 10 % (w/v) SDS
Fixing Solution	50 % (v/v) ethanol, 10 % (v/v) acetic acid
Staining Solution	0.25 % (w/v) Coomassie Brilliant Blue, 10 % (v/v) ethanol, 10 % (v/v) acetic acid
Destaining Solution	10 % (v/v) acetic acid

2.5.3 Differential scanning fluorimetry

Protein stability under various conditions was explored using differential scanning fluorimetry (DSF). This method is able to measure the melting or unfolding temperature of proteins through the binding of the fluorescent dye SYPRO Orange (Invitrogen) to hydrophobic residues located within a protein structure [63]. A basic fluorescence intensity is excited by light of 492 nm. As a protein unfolds, increased hydrophobic contacts detected by the dye and the rate of this detection reach their highest point. The highest rate of change of fluorescent signal at 610 nm is synonymous with the melting temperature (T_m) of the protein (Fig. 2.2) [63-65].

DSF is known as a highly sensitive screening method since the relatively high wavelength for excitation for SYPRO orange (the hydrophobic dye used), near 500 nm, also decreases the likelihood that any small molecule would interfere with the optical properties of the dye and cause, for example, quenching of the fluorescence intensity [63].

Two concentrations of dye (100 x and 200 x) were made up by diluting the supplied solution (SYPRO Orange) in Buffer A. Protein samples for testing were added to each dye mix to a concentration of 1 mg/ml, and diluted further in screening buffer (containing molecules or at conditions intended for protein T_m investigations) at a 1:10 ratio. Aliquots (20 µl) were transferred to a 96-well plate (Strategene) in triplicate, and solutions mixed by centrifugation of the plate (1000 rpm, 1 min). The plate was heated from 25 to 95 ˚C at a rate of 1 ˚C/min in a real-time Q-PCR machine (Mx3005P, Strategene).

Data output containing the rate of change of fluorescence intensity (dR) at a given temperature was provided in a Microsoft Excel format for analysis.

2.5.4 Isothermal titration calorimetry

Isothermal titration calorimetry (ITC) can monitor the formation or dissociation of molecular complexes by measuring the energy needed to offset the heat of reaction. In short, a ligand is injected in aliquots into the sample solution containing protein, and the heat either released (exothermic reaction) or taken up (endothermic reaction) is measured by determining the power required to maintain a constant temperature with respect to a reference solution. As the titration progresses and the binding sites become saturated, the

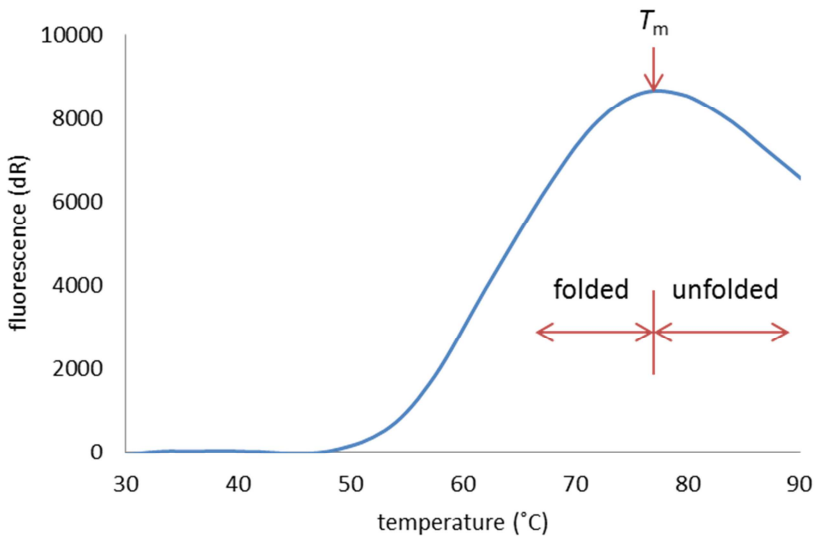

Fig. 2.2. Representation of a melting curve using DSF. Melting temperature (T_m) of the protein (Lsm) is synonymous with the highest point of the curve. This is where the rate of change of fluorescence signal is at its highest. To the left of this point the protein is folded, but to the right it is denatured.

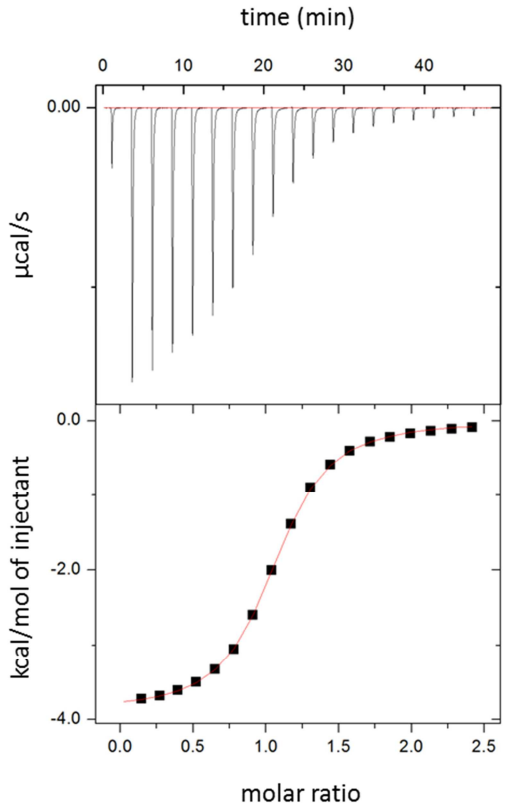

Fig. 2.3. ITC graph of standard calibration reaction. $CaCl_2$ (5 mM) was injected into EDTA (0.4 mM) in calibration buffer (10 mM MES buffer, pH 5.6). Fitting the sigmoidal curve gives N = 1.0, K_d = 7.0 x 10^4, ΔH = -4.0 x 10^3, and ΔS = 9.0.

reaction heats tend to zero [66-69]. The only downfall with this method is that it requires a large amount of purified protein, and identical protein and ligand buffer conditions.

ITC measurements were made using a MicroCal Auto-iTC200 (GE-Healthcare, Fig. 2.3). For analysis of ***Ab*-WbjB** samples, proteins were dialysed (1 - 2 ml in Cellu Sep T1 membranes; MWCO 3,500) in Buffer T for 24 h with 4 total changes of buffer. Protein samples were then diluted to 20 µm in the final aliquot of buffer (ITC buffer). Ligands for testing (1 mM in ITC buffer) were injected in aliquots (0.5 µl first injection, followed by 2 µl injections) into the thermal cell containing protein. Results were analysed using Origin 7 software (Microcal Inc., U.S.A).

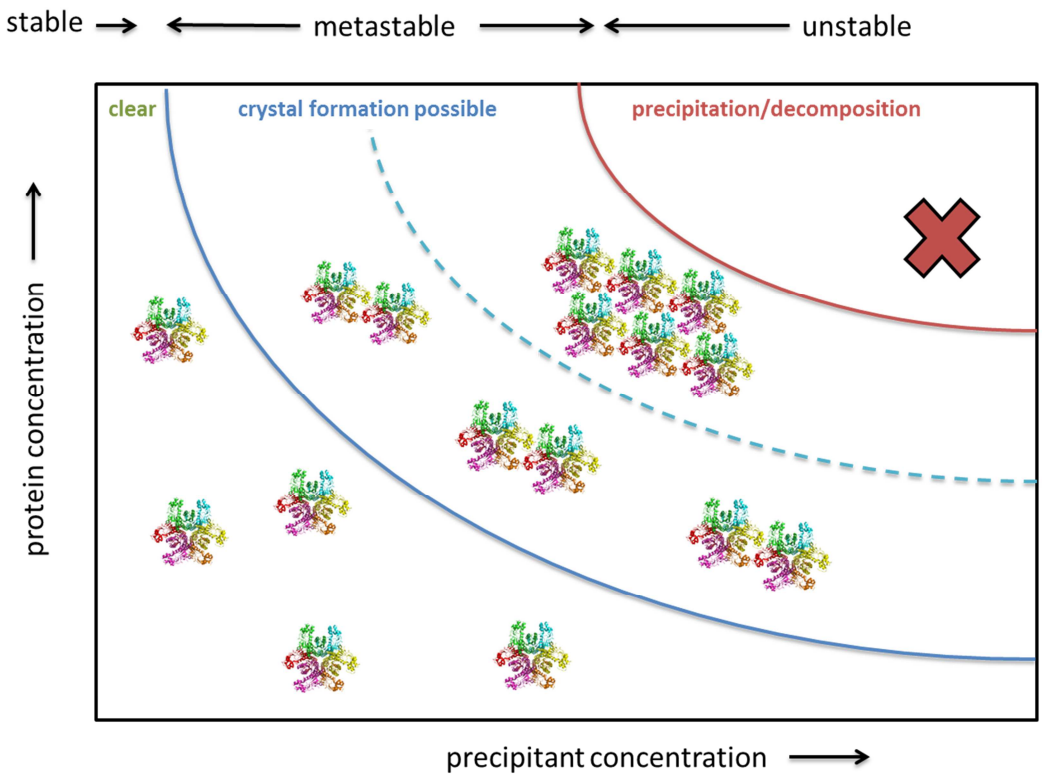

Fig. 2.4. Nucleation zones in protein crystallisation. Solution remains clear until solution becomes metastable resulting in either heterogeneous nucleation (microcrystals or other precipitants) or homogeneous nucleation (stable crystallisation nuclei). If solution becomes unstable the protein precipitates out and can degrade. Figure adapted from [71].

2.6 Protein crystallisation

Protein crystals form when super saturation slowly builds up in a closed system, reducing protein solubility and resulting in ordered, crystalline material (Fig. 2.4) [70]. These crystals can then be harvested and placed in an X-ray beam line in order to attain a diffraction pattern. The extent to which the crystal diffracts, with well-ordered crystals diffracting to a high resolution, determines how detailed the final electron map will be and subsequently how accurate the resulting protein model will be [71, 72].

The goal of my work was to provide better diffracting crystals of ***Ab*-WbjB** than those previously obtained by Dr. Shah [16]. As sparse-matrix screening [73] had previously been carried out by Dr. Shah, there was no need for added screens to determine conditions in which ***Ab*-WbjB** formed crystals. My particular focus was to co-crystallise ***Ab*-WbjB** with bound cofactor and substrate analogue. Condition optimisation on protein samples was carried out in a hanging-drop vapour diffusion format (24-well VDX Plate with sealant, Hampton Research). Two trays were set up containing different buffer conditions (200 mMNaCl, 100 mM HEPES buffer, 25 % PEG3350, 20 % glycerol (Crystal buffer), pH 5.6 and 8.0), but identical cofactor and ligand concentrations (see section 3.3). Protein (1 µl) was combined with Crystal buffer (1 µl) on each cover slip and sealed in place with silicon over buffer reservoirs (500 µl). Each tray was left at room temperature and examined under microscope at a 2 – 3 day frequency for one month.

For crystal harvesting, cover slips were removed and the original protein drop combined with its mother liquor (30 µl). Crystals (see section 3.3) were harvested using a loop attached to a steel pin and magnetic base (Hampton Research) and dipped directly into liquid nitrogen for cryocooling [74, 75]. There was no need for cryoprotectant as the mother liquor included 20 % glycerol. As there was no in-house defractometer available, all crystals were stored in liquid nitrogen for transport and then exposed to the Synchrotron beamline (Melbourne). Once resident at the beamline, crystals were visually inspected for diffraction limit (highest resolution), presence of ice rings, spot separation and sharpness of spots. For synchrotron data collection, crystals were rotated around a single axis by small successive increments (0.5 - 1˚) while exposed to the X-ray beam and a diffraction image or frame was recorded

during each rotation increment [76]. All data collection at the synchrotron was carried out by Dr. Shah.

Chapter 3: Production and buffer characterisation of recombinant forms of *Ab*-WbjB

3.1 Preparation of recombinant *Ab*-WbjB

In order to obtain pure samples of ***Ab*-WbjB** for functional characterisation, recombinant production was carried out in a conventional bacterial host by autoinduction (section 2.3). This protein is encoded by the gene *fnlA* found in a genomic island in the D1279779 community strain of *Acinetobacter baumannii*. The gene *fnlA* had been engineered to code for a hexa His-tag at the N-terminus, enabling protein purification by capture through immobilised metal affinity chromatography (IMAC). With availability of the gene cloned into the expression host (HC_***Ab*-WbjB** pLysS), the protein product was readily obtained from cultures grown in shaker flasks.

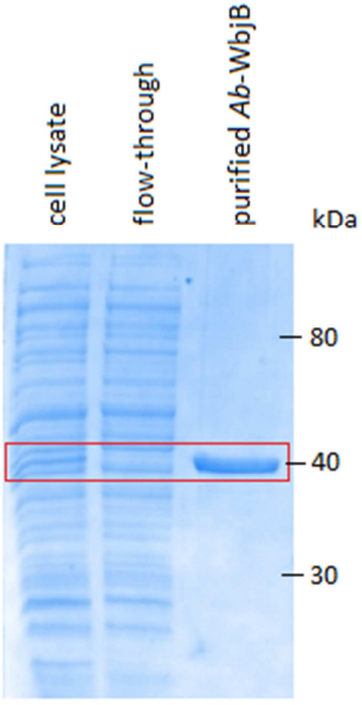

Fig. 3.1. SDS-PAGE of protein samples during purification of His-tagged ***Ab*-WbjB**. Lanes show protein profiles following I) cell lysis by sonication/freeze thaw, II) eluent from His-trap (GE-Healthcare) running in Buffer A, 50 mM imidazole, and III) protein obtained in Buffer A, 500 mM imidazole. Gel is stained with Coomassie Brilliant Blue.

Cells growing in 2 L baffled flasks were pelleted by centrifugation and lysed using a freeze-thaw cycle and sonication. Cell lysate (in Buffer A), was loaded onto an IMAC column and washed with Buffer A containing 50 mM imidazole. ***Ab*-WbjB** (with engineered His-tag) bound to the column so that unwanted cytosolic proteins could be removed by this wash step. The target protein was eluted with Buffer A containing 500 mM imidazole, which resulted in pure ***Ab*-WbjB** protein samples of high concentration seen in Fig. 3.1. This was evident by the single band seen on SDS-PAGE gel. Following some optimisation of buffer conditions (see below), production was possible to approximately 25 mg/ml.

3.2 Stabilisation of *Ab*-WbjB in solution

Initial buffer conditions for the purification protocol of ***Ab*-WbjB** resulted in samples at pH 7.5 (10 mM HEPES buffer) and moderate salt (300 mM NaCl). These conditions were derived from our laboratory's previous handling of ***Ab*-WbjB** [16], but did not appear to give rise to optimal protein stability. Sample protein concentrations, as determined by UV spectroscopy, would drop to very low values over a matter of days, even when proteins were stored at -80 ˚C.

In previous work with other extended short-chain dehydrogenase/reductase enzymes (SDRs), buffer conditions have varied greatly. In the case of FlaA1 from *Helicobacter pylori*, protein samples were purified at neutral pH and very high salt concentration (pH 7.0, 1M NaCl) [49], but with CapE from *Staphylococcus aureus*, samples were purified in basic conditions with low salt (pH 9.0, 30 mM NaCl) [51]. As it appeared necessary to determine the optimal conditions for stability of ***Ab*-WbjB**, a broad buffer screening was carried out.

An effective method that can be used to optimise solution conditions for a specific protein involves measurement of thermal stability assessed at different salt and different pH conditions [65]. Stability of ***Ab*-WbjB** was therefore measured using differential scanning fluorimetry (DSF), which measures the temperature at which proteins unfold (melting temperature, T_m). DSF is an excellent platform to screen for conditions that stabilize proteins, owing to the small amounts and low concentrations of protein required, and its ability to measure 96 samples at once [65].

As buffer conditions for CapE and FlaA1 were so varied, it was decided that a wide variety of salt concentrations and pH conditions would be tested in order to determine optimal buffer conditions for ***Ab*-WbjB**. Salt concentrations of 50 to 300 mM and pH 4.0 to 9.0 were chosen for this purpose. Protein samples of 0.1 mg/ml containing 1 mM NADP were tested against a combination of these conditions.

Fig. 3.2 shows traces for protein samples scanned up to 85 ˚C, as monitored by the excitation of SYPRO orange through a pH range of buffers. At pH of 8.0 and 9.0, the protein displayed a clear folded to unfolded state transitions with a T_m of 74 ˚C. However, at a pH less than 5.0, ***Ab*-WbjB** behaved as already denatured, with no features in DSF response across the temperature gradient. Changing salt concentration made no difference to the stability of ***Ab*-WbjB**, as T_m remained constant between concentrations of 50 to 300 mM NaCl. For example, at pH 8.0, T_m of the protein remained at 74 ˚C independent of salt concentration.

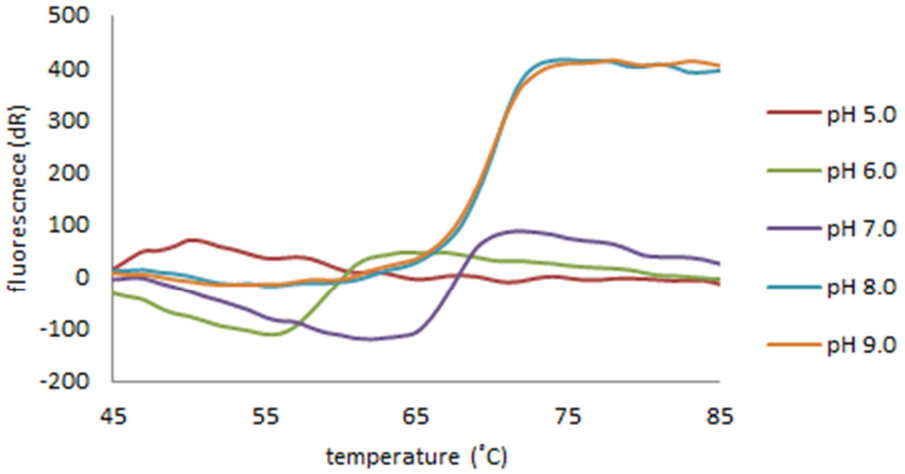

Fig. 3.2. Thermal stability of ***Ab*-WbjB** as detected by DSF under different pH and salt conditions. Protein stability at 300 mM NaCl and pH values from 5.0 to 9.0 (176 mM sodium acetate buffer, pH 5.0; 500 mM MES buffer, pH 6.0; 500 mM HEPES buffer, pH 7.0 and 8.0; 500 mM glycine buffer, pH 9.0). 100x SYPRO orange dye mix was added to 1 mg/ml protein sample and diluted 1:10 in screening buffer.

Based on these results, it appears that ***Ab*-WbjB** requires basic solution conditions above pH 8.0 for optimum stability. This is consistent with the pI value of ***Ab*-WbjB** ,pI 5.9, indicating that the protein is more stable with an overall negative charge. This is very similar to the case of the yeast SDR, CapE, which has pI 5.5 and has been handled at pH 9.0 [48]. As these SDRs sequester their cofactor, nicotinamide adenine dinucleotide phosphate (NADP), from growth conditions, the buffer conditions may influence protein stability through favouring a bound state of this cofactor (Fig. 3.3). There is also the possibility that active site chemistry is stabilised by these conditions.

3.3 Redox control of *Ab*-WbjB quaternary structure

***Ab*-WbjB** contains three Cys residues, two of which are involved in a disulphide bond (Cys121 - Cys160). This leaves six unpaired Cys residues (Cys89) in a hexameric form of the protein. As Fig. 3.3 shows, these are located very near to NADP within the cofactor-binding site. Previously in this laboratory, ***Ab*-WbjB** was purified in buffer conditions containing the reductant *tris*(2-carboxyethyl)phosphine (TCEP, 50 mM) [16].

Almost immediately my studies showed that solutions of ***Ab*-WbjB** were not stable unless this reducing agent or DTT was present. Analysis of my protein samples by size exclusion chromatography (SEC) showed that the quaternary state of ***Ab*-WbjB** was affected by TCEP. The differences of quaternary states between reducing and non-reducing conditions can be seen in Fig. 3.4. With TCEP present, a single species elutes from a Superdex 200 10/300 GL matrix at 12.7 ml. This gives a native mass measure of 290 kDa and has been attributed to the presence of a hexamer of the 40 kDa ***Ab*-WbjB** monomer, consistent with the quaternary complex depicted in Dr. Shah's crystal structure (Fig. 3.3). Without reductant present in the running buffer, the protein predominantly elutes at 14.1 ml on the same SEC matrix, consistent with a native mass of 110 kDa, possibly for a dimeric or trimeric form. However, as ***Ab*-WbjB** is known to be a trimer of dimers, it is most likely that the predominant species is a dimer.

Given that a reducing agent favours the larger oligometric form of ***Ab*-WbjB**, it is unlikely that the alteration in species is mediated by the redox state of Cys89. SDR enzymes utilise a tightly bound NAD(P)(H) cofactor, which stays attached and undergoes different redox state

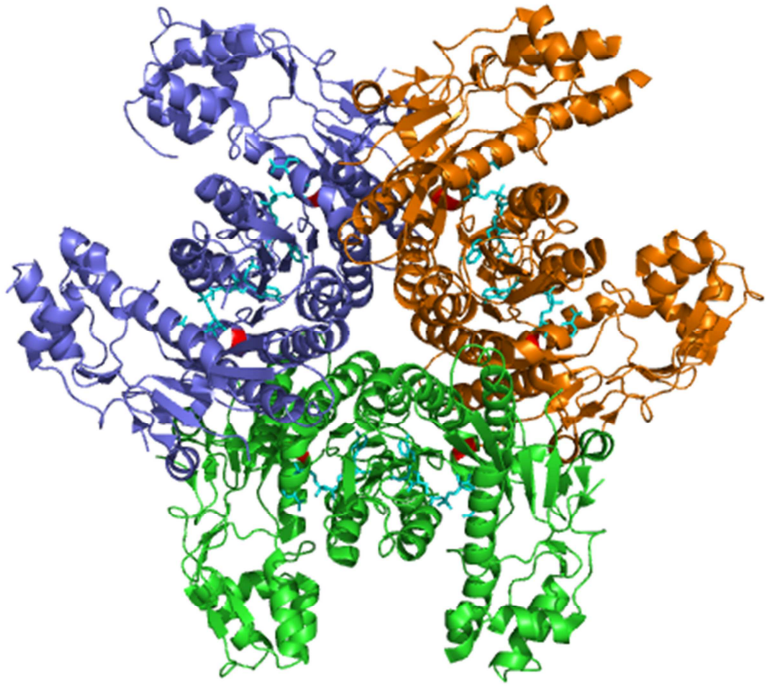

Fig. 3.3. Crystal structure of hexmeric ***Ab*-WbjB**. ***Ab*-WbjB** is a trimer of dimers as denoted by each colour. NADP (cyan) can be seen in each monomer in relation it the single Cys residue (Cys89, red).

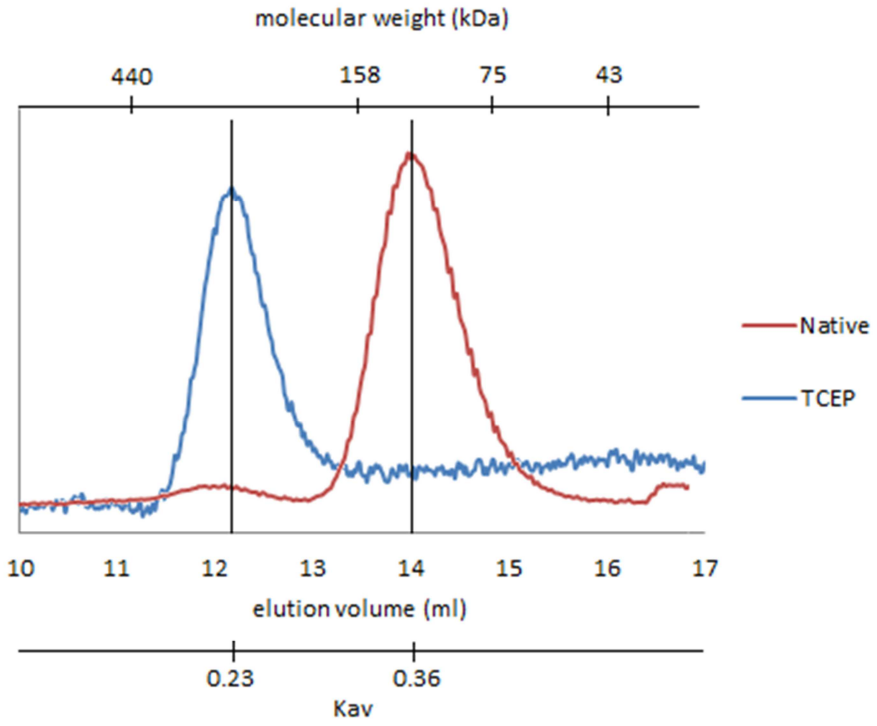

Fig. 3.4. SEC trace of ***Ab*-WbjB** on Superdex 200 10/300 GL matrix in Buffer A with and without reducing agent TCEP (0.5 mM). Error rate of SEC is approximately 10-15 %.

changes during the reaction cycle [77, 78]. Thus it is likely that the reductant alters the cofactor environment to change the oligometric state of the protein. A similar dimeric state has been seen in homologous FlaA1 [49].

3.4 Creation of active site mutants

The substrate-binding site of SDRs shows more variation than the cofactor-binding site, presumably due to tuning of enzyme specificity. However, catalytic activity relies on a conserved triad of Ser, Tyr, and Lys [40, 45], for extended SDRs generally seen as a sequence motif of YxxxK [77]. In ***Ab*-WbjB**, (as with CapE) [48], this catalytic triad utilises Ser123, Met134, and Lys138, with a Met residue instead of the canonical Tyr. Tsumoto has proposed that the Met residue found in the binding pocket of CapE is part of a novel latch structure, a mobile loop containing residues 287–309, that regulates access of substrate to its nearby binding pocket [48]. Although this latch was not directly depicted in the crystal structure of ***Ab*-WbjB** due to dynamic mobility, it is still speculated to be present [16].

In order to probe distinct chemical features related to the putative substrate site in ***Ab*-WbjB**, active site residues of this enzyme sequence were selected for mutation. In each mutant, bulk groups known to be active in each sidechain (SH and OH groups) were replaced with inactive methyl or hydrogen groups in order to destroy possible interactions with substrate or cofactor. In addition to this Met134 was changed to Tyr134 in order to replicate active site chemistry in other SDRs. The reverse mutation has been achieved for FlaA1 (Y141M) in order to observe change in activity, as another SDR (WbpM) with a Met replacing the active site Tyr had been discovered [79]. The only mutant residue not thought to be directly involved in active site chemistry was Cys89. This was chosen due to hypotheses on its involvement in the quaternary structure of ***Ab*-WbjB**. Similar mutations in FlaA1 (C103M) resulted in the protein losing its ability to form a dimer [79]. All of these residues can be seen in relation to NADP and the proposed substrate-binding site in Fig. 3.5.

Primers were designed for these mutants as seen in Table 2.3, and single point mutations in the *flnA* gene were acquired through a PCR thermo cycle. DNA was then transformed into competent cells and successful mutants were selected for on antibiotic agar plates. Further confirmation of mutations was achieved through gene sequencing (Macrogen). Mutant DNA

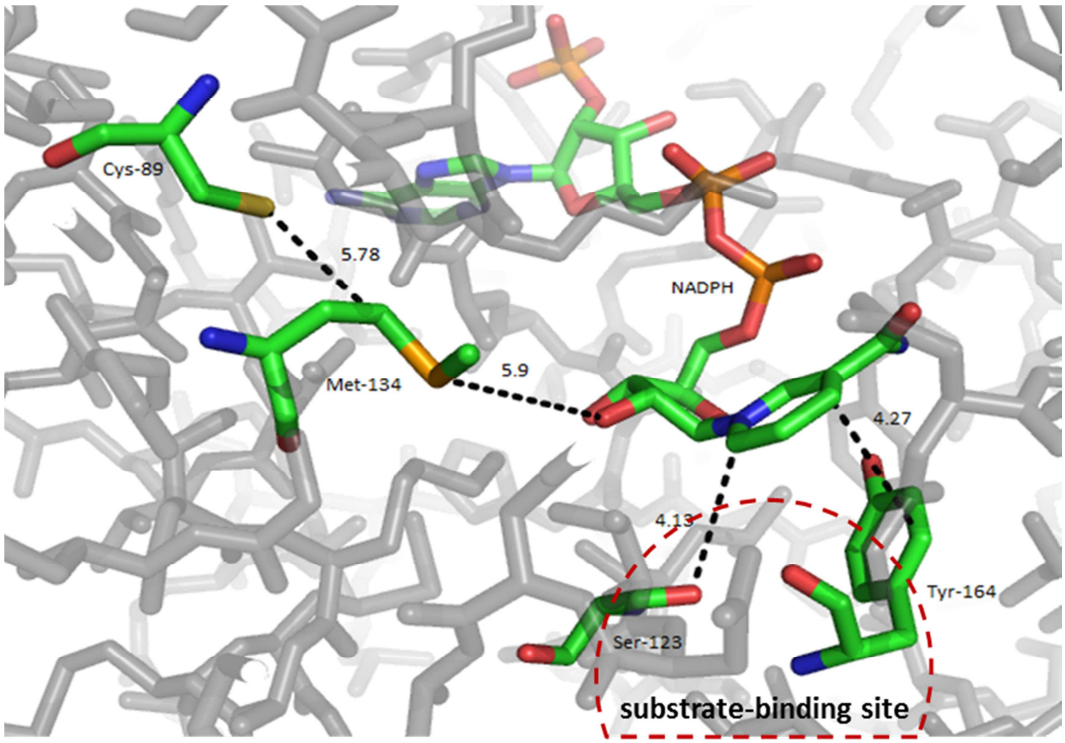

Fig. 3.5. NADPH-binding region within crystal structure of ***Ab*-WbjB**. Specific sidechains chosen for mutagenesis are depicted in relation to NADP. Approximate distances (Å) from the cofactor are displayed except for Cys89 which is adjacent to Met134.

Table 3.1. Site-specific mutants of ***Ab*-WbjB** prepared via quickchange

	verified by sequencing	soluble protein
1. proposed active site role		
S123A	✓	-
M134A	✓	✓
M134L	✓	-
M134Y	✓	-
Y164F	✓	✓
2. possible redox role		
C89A	✓	-

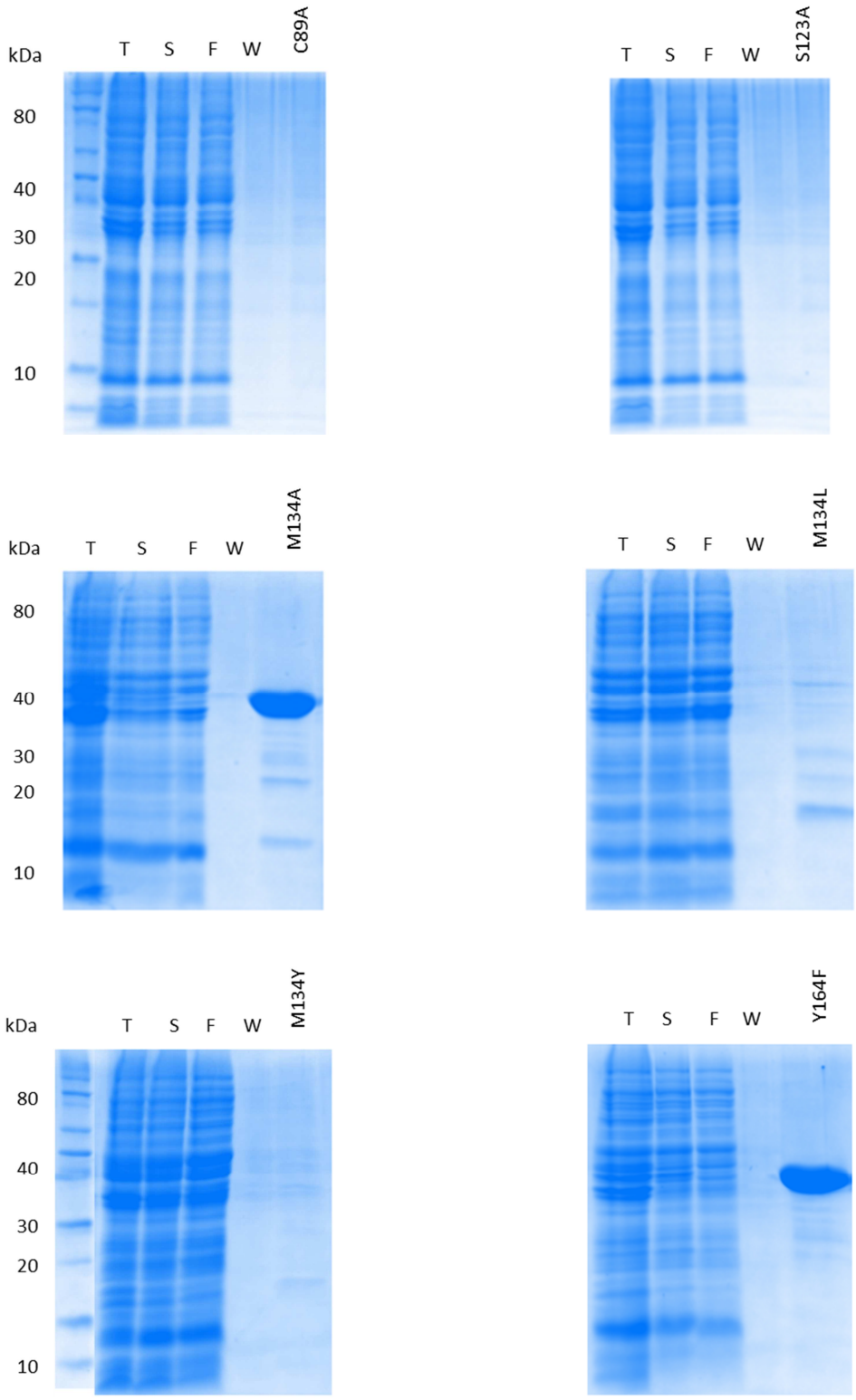

Fig. 3.6. Site directed mutagenesis of active site residues in ***Ab*-WbjB**. Success of the mutants was based on final protein yield after purification. SDS-PAGE gels were run with fractions collected during the purification process (T = total lysate, S = soluble fraction, F = IMAC flow-through, W = column wash).

was then transformed into an expression host, and protein expressed through autoinduction as seen in section 2.3.

It was possible to recover and fully purify the two mutants M134A and Y164F to a concentration of 2 mg/ml or higher as seen in Table 3.1 and Fig 3.6. Failed mutants may have occurred due to overall protein instability after the change in residues, or occlusion of the His-tag resulting in limited or no adsorption to an IMAC column.

Chapter 4: Biochemical annotation of *Ab*-WbjB

4.1 Previous work on *Ab*-WbjB

***Ab*-WbjB** shares a high structural identity with other members of the SDR family. CapE, a capsular polysaccharide-synthesising enzyme from *Staphylococcus aureus* [48], shares a sequence identity of 68%. The protein FlaA1, found in *Helicobacter pylori* is thought to be involved in glycosylation of flagella proteins because of its relation to FlmA and PglF [49, 80, 81], and has 39% sequence identity with ***Ab*-WbjB**. Although the end product of these two related SDR enzymes is predicted to serve different functions, their substrates sites appear to be similar. CapE has been shown to bind UDP-6N3-GlcNAc, whereas the structure of FlaA1 was solved with UDP-GlcNAc occupying the active site (Fig. 4.1, A) [50]. The proposed mechanism for the modification of UDP-GlcNAc in FlaA1 can be seen in Fig. 4.2.

It is known that SDRs constitute a large family of NAD(P)(H)-dependent oxidoreductases and that a lot of SDR crystal structures include molecules of NADP [77]. Epimerase SDRs contain a tightly bound NAD+ molecule, which stays attached and undergoes different redox state changes during the reaction cycle. This is thought to apply in a similar way to other types of SDRs. As seen in Fig. 4.1, in the crystal structure of ***Ab*-WbjB**, the cofactor for enzymatic reaction, nicotinamide adenine dinucleotide phosphate (NADP), can be clearly observed bound to the cofactor-binding domain [16]. This was due to sequestration of this molecule from growth media, as no addition of NADP was made to crystallisation components. NADP(H) binding is dictated by the presence of a basic residue within the Gly-rich segment as observed in the SDR family [44]. In the case of ***Ab*-WbjB**, this is provided by Lys7.

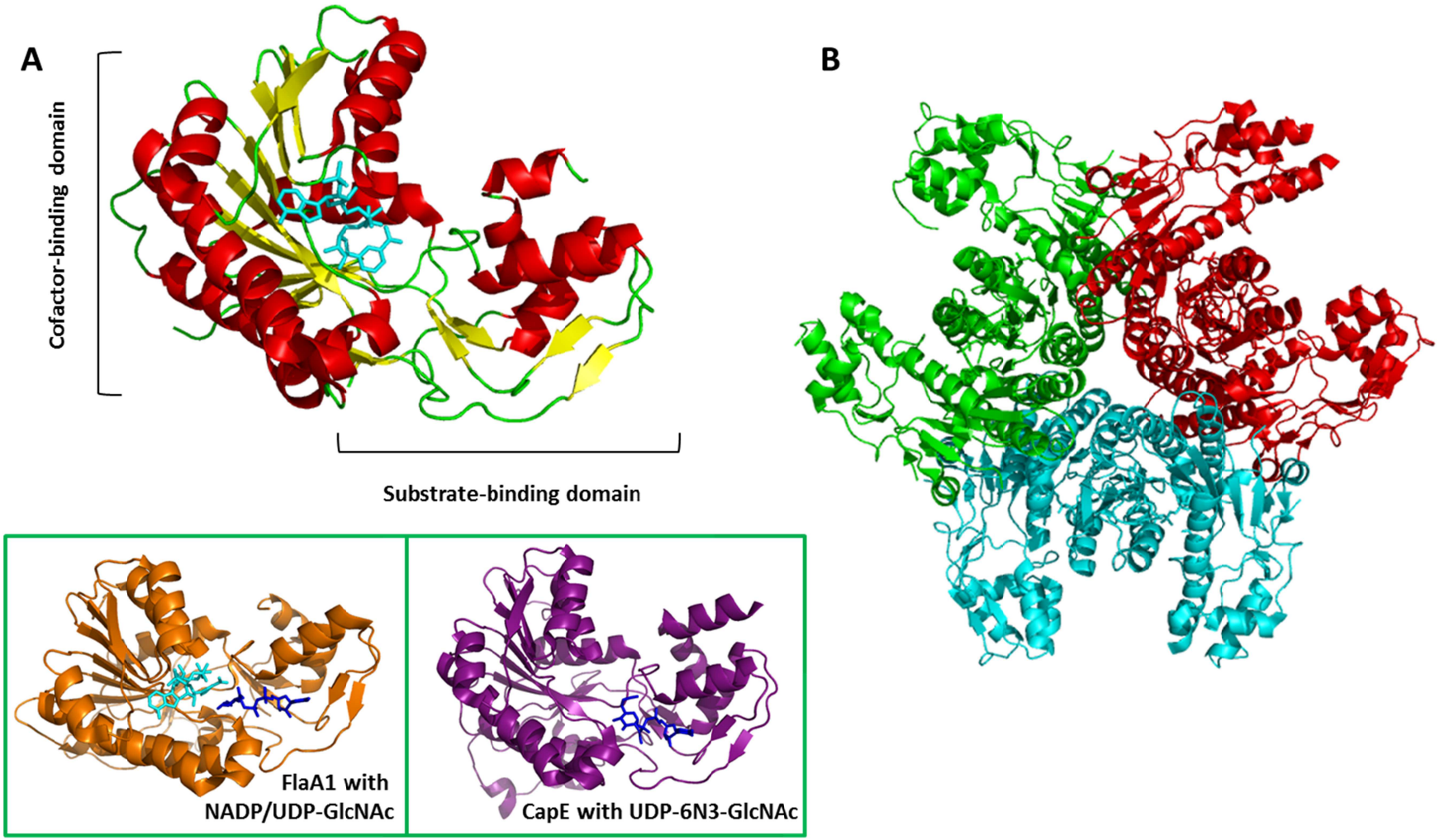

Fig. 4.1. Structure of ***Ab*-WbjB**. (A) Chain A of the full structure showing the position of NADP in the cofactor binding domain and the empty substrate binding domain. Also shown are the structures of FlaA1 and CapE with NADP (cyan) and substrate analogue (blue). (B) Hexameric structure showing the position of each chain . ***Ab*-WbjB** is a trimer of dimers.

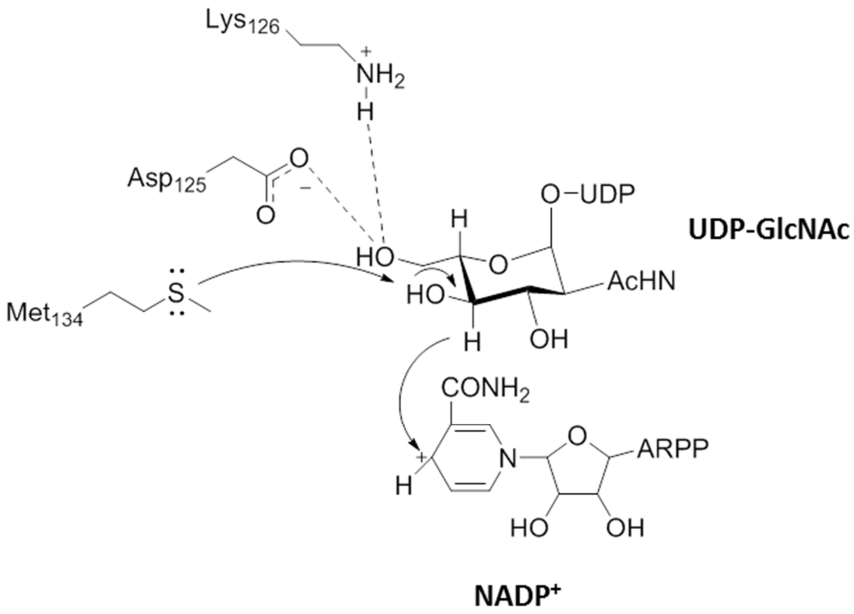

Fig. 4.2. Proposed mechanism for FlaA1 UDP-GlcNAc oxidation with substitution of residues seen in ***Ab*-WbjB** [16]. ARPP is the adenosine ribose pyrophosphate moiety of NADP. Met134 is replaced with Tyr141 in FlaA1.

Tight binding of NADP was observed in similar locations within CapE and FlaA1 engaging Lys28 in CapE and Lys25 in FlaA1 (Fig. 1.5) [48, 50].

Although the cofactor-binding site common amongst the SDRs is well understood and characterised, there is a wide variety of requirements for the diverse group of substrates engaged. Common to all SDR members is the ability to interconvert substrates containing hydroxyl/oxo groups [77]. So, even though it seems that the substrate site within ***Ab*-WbjB** has capacity to bind UDP-GlcNAc given the single crystal structure solved, there is doubt as to the relationship between this sugar derivative and the biological substrate for which ***Ab*-WbjB** has evolved. One of the goals of this research was to identify a substrate analogue for ***Ab*-WbjB** and to allow for its capture in a non-active state and for new crystals to be grown. In addition to this, studies into the specificity of the substrate-binding domain chemistry were carried out to begin to illuminate active site mechanisms.

4.2 Role of NADP in *Ab*-WbjB stability

It has been shown in epimerase SDRs that binding of UDP to the nucleotide-diphosphate domain enhances reactivity of NAD+, suggesting cooperative behaviour between the UDP-binding domain and the central catalytic domain [77]. This would in turn suggest that without full occupation of cofactor-binding sites in SDRs, substrate binding would be compromised. In order to probe possible stabilising effects that NADP could have on ***Ab*-WbjB**, differential scanning fluorimetry (DSF) was used. Results from multiple DSF experiments seen in Fig. 4.3, 4.4, and 4.5 shows that the addition of excess NADP (a protein to NADP ratio of 1:30,000) increases the stability of ***Ab*-WbjB**, with increases of T_m anywhere from 3 to 5 ˚C. This suggests that the natural amount of NADP available during culture conditions is not enough to fill all six subunits of ***Ab*-WbjB** seen in Fig 4.1 (B), and therefore the addition of excess NADP (1 mM) fills all cofactor-binding sites and fully stabilises the protein.

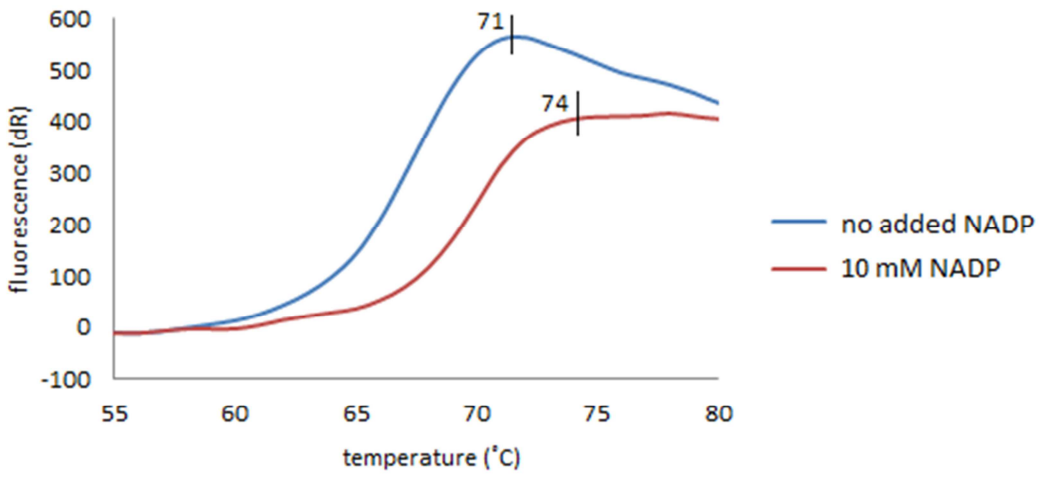

Fig. 4.3. Effect on ***Ab*-WbjB** with the addition of excess NADP (1 mM). Native ***Ab*-WbjB** protein samples (purified in Buffer A) contain no excess NADP and displayed a T_m of 71 ˚C. ***Ab*-WbjB** after addition of 1 mM NADP (a protein to NADP ratio of 1:30,000) had an increase in T_m to 74 ˚C.

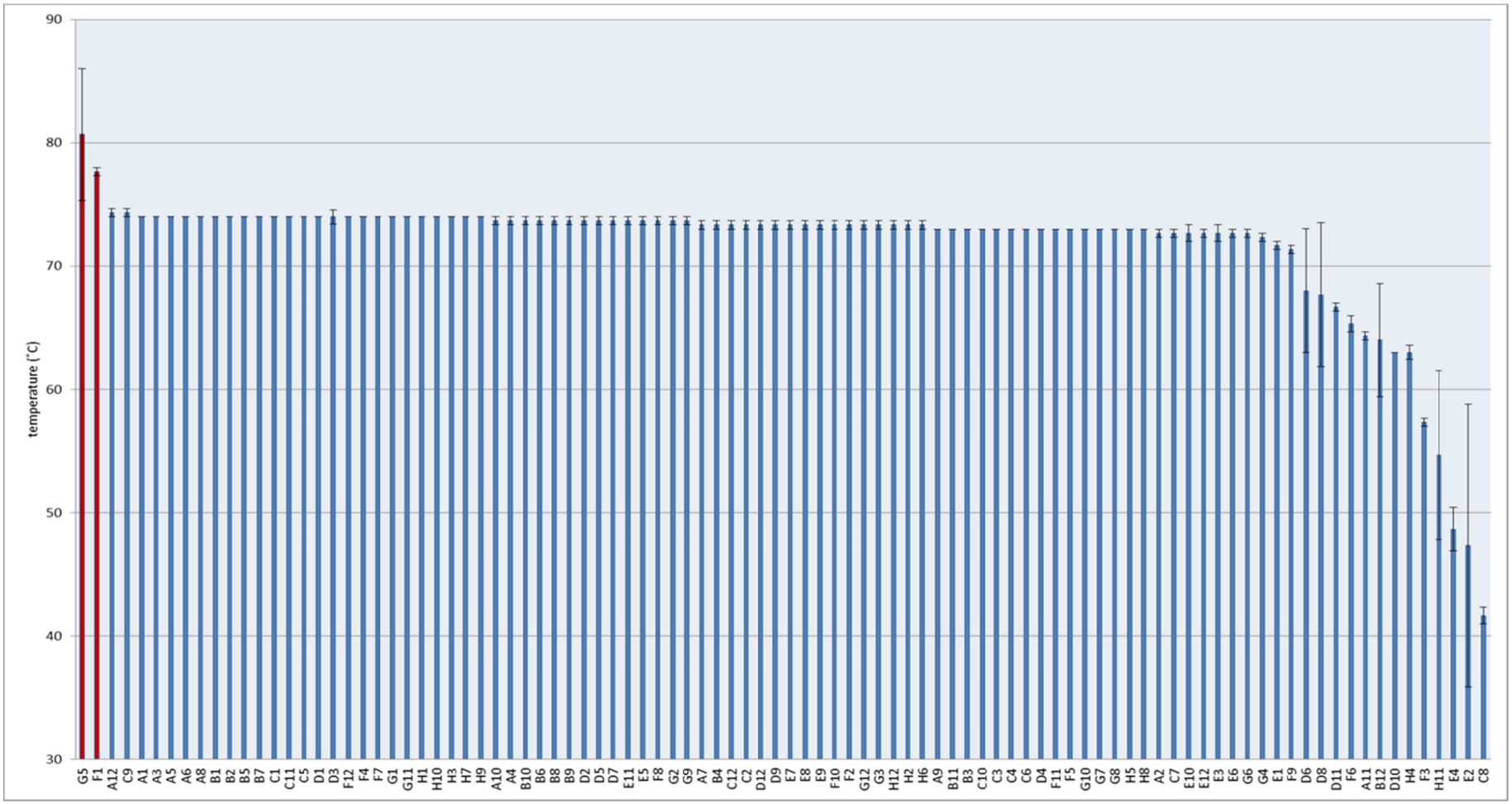

Fig. 4.4. DSF screen for possible **Ab-WbjB** substrates using screens of the Hampton 'Silver Bullet' range. **Ab-WbjB** was combined with each of the 96 conditions in a 96-well plate and monitored using DSF. Experiments were carried out in triplicate. No NADP was added to buffers.

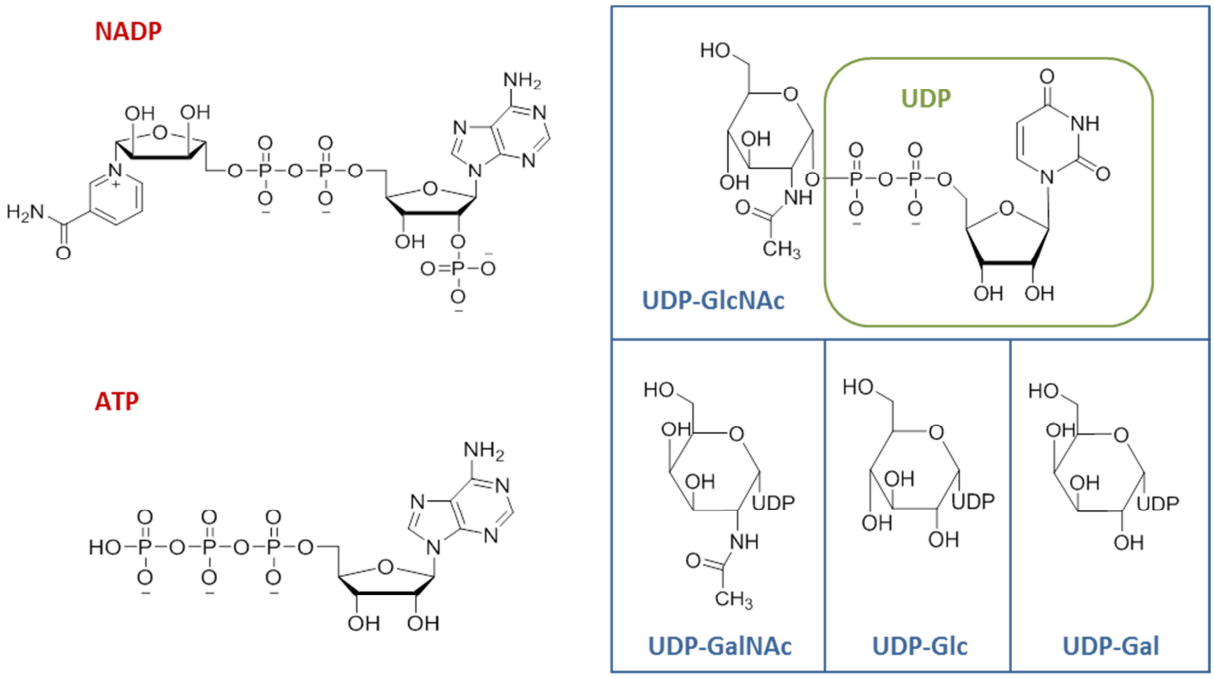

Fig. 4.5. Molecular structures of possible cofactors and substrates for ***Ab*-WbjB**. Cofactors NADP and ATP are grouped separately from possible substrate nucleotide sugars. The structure of uridine dosphate (UDP) is drawn out in full.

When using isothermal titration calorimetry (ITC), this cooperative effect between the substrate-binding domain and cofactor-binding domain was further supported. ***Ab*-WbjB** would only bind substrate in the presence of excess NADP. When NADP was not added, meaning only a portion of cofactor-binding sites were occupied, binding events were not seen (results not shown).

4.3 Substrate chemistry search for *Ab*-WbjB

As a starting point for determining a possible substrate for ***Ab*-WbjB**, large-scale molecular screening was used. A commercial screening kit containing a suite of organic molecules, salts, and metals, based on previous crystallisation success was used to probe stabilising effects on ***Ab*-WbjB** protein samples. The commercial additive screen (Silver Bullets Screen, Hampton Research), is more commonly employed for the optimization of protein crystals.

***Ab*-WbjB** protein samples were mixed with the 96 different conditions at a 1:10 dilution in a 96-well plate. Most conditions trialled (81 out of 96) did not affect the stability of ***Ab*-WbjB**. Two conditions favourably increased T_m of ***Ab*-WbjB** above 74 ˚C as depicted in Fig. 4.4. The

most stable condition increased T_m to 81 ± 5 ˚C and contained UDP-*N*-acetyl-D-glucosamine (UDP-GlcNAc) (Fig. 4.5). Although additional components were present (riboflavin 5'-monophosphate, maleic acid, pyridoxamine, and acetylcholine), it was postulated that UDP-GlcNAc was most likely the ligand to cause this effect.

A second condition also resulted in an increased T_m (78 ± 1 ˚C) and can be seen in Fig. 4.4. The well contained NADP, ATP, N-acetyl-D-galactosamine (GalNAc), and gentamicin. This temperature increase was likely due to the presence of NADP and ATP, but could also be due to GalNAc. Increased protein stabilisation of ***Ab*-WbjB** by NADP has been explained above. As ATP has a similar chemical structure to NADP (Fig. 4.5), it could well bind at the cofactor site, so stabilising through similar molecular effects. Binding of a compound similar to GalNAc (GlcNAc) was later tested, seen in Fig. 4.7, but was found to display no evidence of binding to ***Ab*-WbjB**.

Two major groups of destabilising conditions contained amino acids and heavy metal chloride salts. The amino acids found in destabilising screens contained polar uncharged side chains (Tyr, Ser, Thr, Asn, and Gln) and electrically charged side chains, both positive and negative (Arg, His, Lys, Asp, and Glu). These residues may have adversely interacted with surface residues in ***Ab*-WbjB** through ionic and hydrophilic interactions altering protein fold properties. Heavy metals are known to bind to cysteine groups and disrupt disulphide bonds [82], and ***Ab*-WbjB** contains six disulphide bonds when in hexameric form (Cys121-Cys160).

As cocktail screens contained multiple components, conditions that increased T_m of ***Ab*-WbjB** were investigated in more detail individually. The compounds chosen, ATP, NADP, and four UDP sugars (UDP-GlcNAc, UDP-GalNAc, UDP-Glc, UDP-Gal), were hypothesised to show the greatest DSF response. Fig. 4.6 shows that NADP and ATP increased T_m by 3 ˚C (76.5 ± 1 ˚C) and 1 ˚C (74.5 ± 0.5 ˚C) respectively. However, a significant increase in T_m could not be produced when screening UDP sugars. It has been seen that binding of UDP sugars only occurs at the dinucleotide portion (Fig. 4.5), facilitating the rotation of the sugar (sometimes up to 180 ˚), and allowing modification by the enzyme [77, 83, 84]. This loose binding of substrate would not increase the stability of ***Ab*-WbjB**, and therefore did not merit a DSF response.

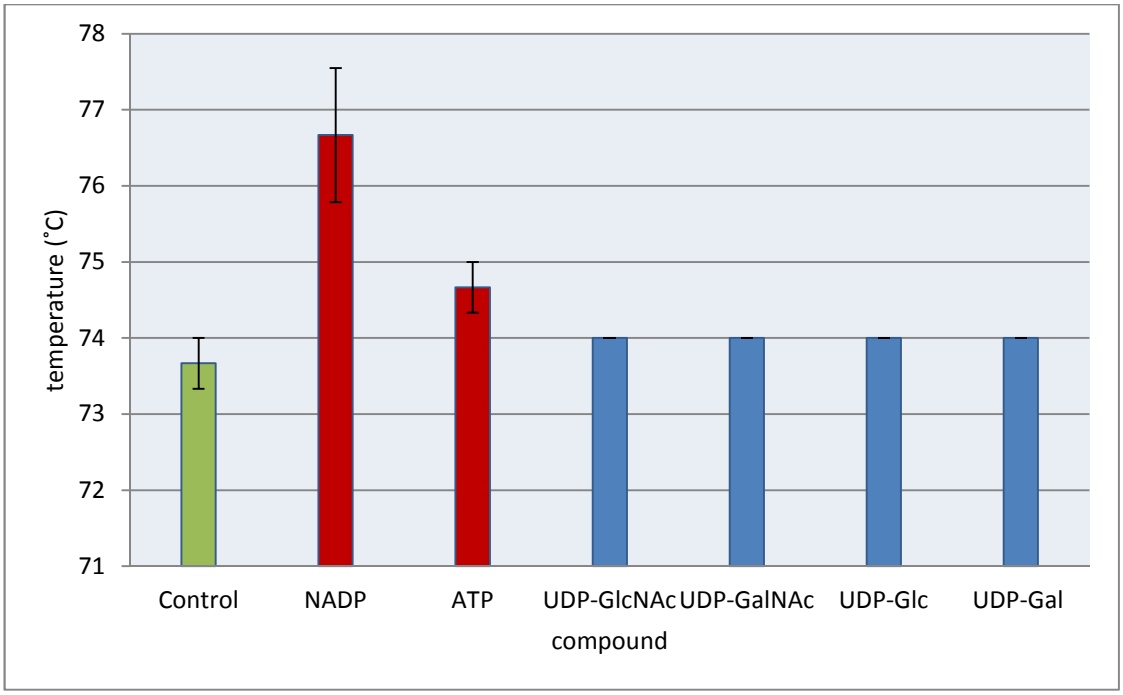

Fig. 4.6. DSF screening of additives seen to increase stability of ***Ab*-WbjB** in cocktail solutions. All compounds were added to a 1 mM concentration in Buffer A with 100 x dye. Experiment was carried out in triplicate.

For further investigation into binding of UDP sugars to ***Ab*-WbjB**, isothermal titration calorimetry (ITC) was chosen in order to observe specific binding events rather than global stability effects. ITC can monitor the formation or dissociation of molecular complexes by measuring the energy needed to offset the heat of reaction (see section 2.5.4).

Different structural iterations of UDP-GlcNAc were compared in order to determine which chemical moieties were necessary for binding. Four candidate ligands were tested, namely UDP-GlcNAc, UDP-Glc, GlcNAc, and glucosamine. The structures of these compounds and ITC results are seen in Fig. 4.7. Binding to ***Ab*-WbjB** resulted in a change in enthalpy (ΔH) of -800 ± 180 kcal/mol for UDP-GlcNAc, -780 ± 400 kcal/mol for UDP-Glc, -150 ± 60 kcal/mol for GlcNAc, and 220 ± 250 kcal/mol for glucosamine. Both UDP-GlcNAc and UDP-Glc showed an exothermic change in ΔH consistent with good binding to ***Ab*-WbjB**. GlcNAc exhibited little change in ΔH, suggesting little or no binding. Glucosamine displayed a positive change in ΔH which represents endothermic binding, extremely unfavourable in any enclosed system.

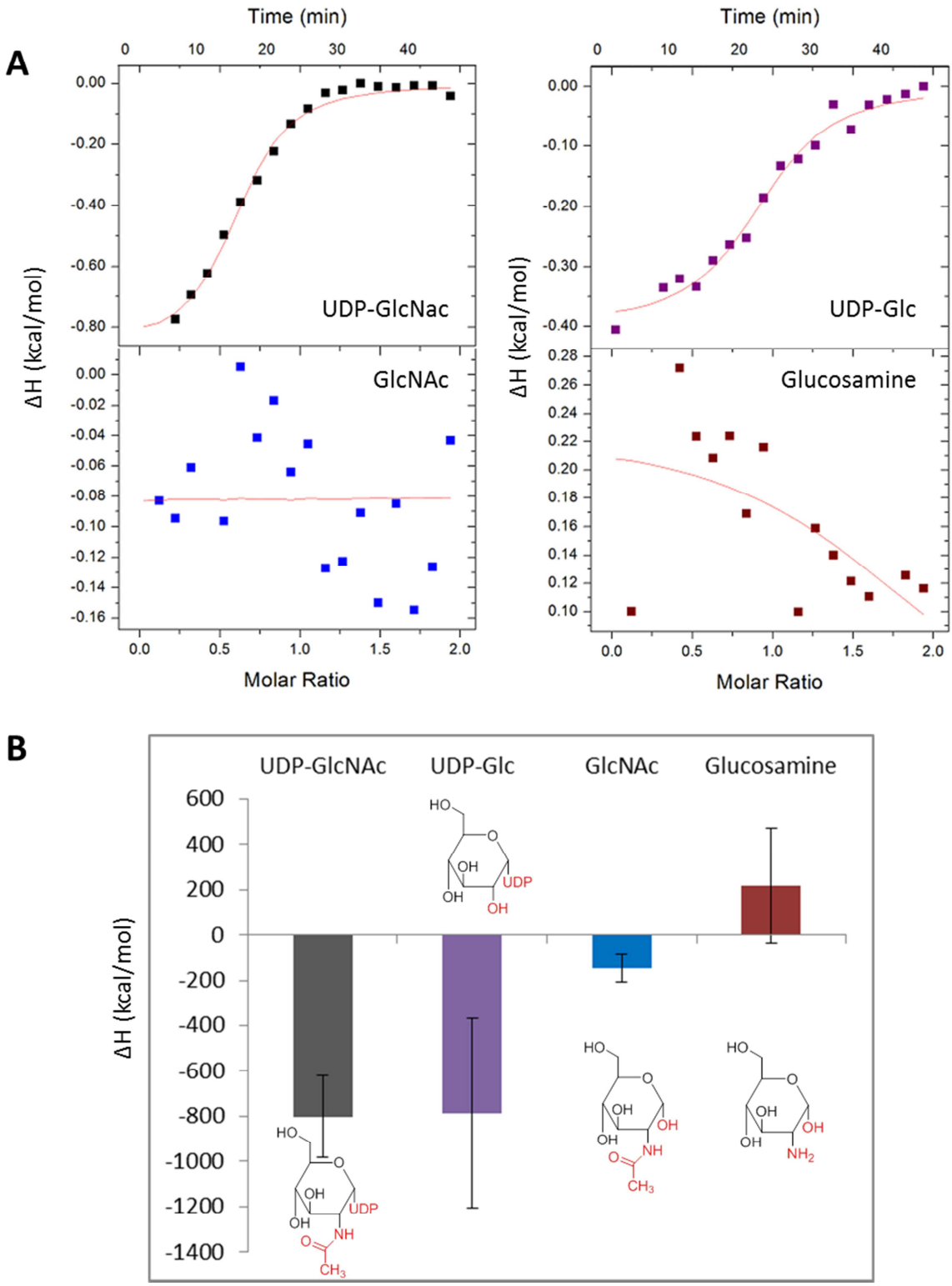

Fig. 4.7. ITC substrate binding. (A) Results for the average binding of ***Ab*-WbjB** to UDP-GlcNAc, UDP-Glc, GlcNAc, and glucosamine. Reactions carried out in Buffer A with 1 mM NADP. Protein concentrations were 20 µM and sugars 1 mM (B) Comparative graph between the enthalpy of binding for each compound with error bars shown. The structure for each compound is also shown.

These results imply that the dinucleotide portion of sugars used was absolutely necessary for decent binding to ***Ab*-WbjB**. The exothermic binding of UDP-GlcNAc and UDP-Glc supports the theory that epimerase SDRs bind the UDP part of UDP sugars and leave the sugar portion open for movement [77, 85]. This can also be seen in Fig. 4.8 which shows the active site of the CapE enzyme. The UDP portion of the inhibitor UDP-6N_3-GlcNAc comes in very close proximity to the active site residues Lys126 and Glu257, but the sugar portion remains free from hindrances to movement. ITC results also suggested that the removal of an acetyl group affects binding, as reactions involving GlcNAc were more favourable than those with glucosamine. However, the reason for this cannot be visualised in the CapE structure below (Fig. 4.8).

4.4 Functionality of key active site residues

With ***Ab*-WbjB** mutants (M134A and Y164F) available for testing, these could also be included in measurements for binding efficiency to UDP-GlcNAc. Met134 is thought to play a key role in active site chemistry of ***Ab*-WbjB**, taking part in the oxidation proton relay mechanism seen in Fig. 4.2. Tyr164 was mutated in order to see if it had taken on any of the roles held by active site tyrosines in other SDRs. Isothermal binding results in Fig. 4.9 show that mutation of these two residues did have an effect on binding of UDP-GlcNAc. The mutation Y164F resulted in a drop in ΔH to 25 % of native ***Ab*-WbjB** (-200 ± 80 kcal/mol),whereas M134A only retained 6 % activity (-50 ± 20 kcal/mol). The M134A mutant was also tested for binding to UDP-Glc, GlcNAc, and glucosamine, yielding ΔH values of -200 ± 750, -400 ± 650, and -150 ± 20 kcla/mol, respectively.

In ***Ab*-WbjB**, the Met134 SH group could participate in the proton relay as proposed for FlaA1 (Fig. 4.2). However, its SH group is not as amenable to proton exchange as the OH group of Tyr141 in FlaA1. If Met134 did play this role in proton relay, then the mechanism would no longer be able to proceed when the Met is replaced with Aln. Thus, this loss of binding is consistent with the need for proton exchange at the Met134 location in ***Ab*-WbjB**.

Unfortunately the role of Tyr164 is still not known for ***Ab*-WbjB**. As seen in Fig. 4.8, it does not directly interact with the substrate (UDP-6N_3-GlcNAc), but is a lot closer in proximity to NADP, as seen in Fig. 3.5. As the change of Tyr to an Aln would cause the loss of an OH group, it could affect the stability of NADP and subsequently the stability of the active site. This would result in a loss of binding of UDP-GlcNAc to ***Ab*-WbjB**. Future comparisons on

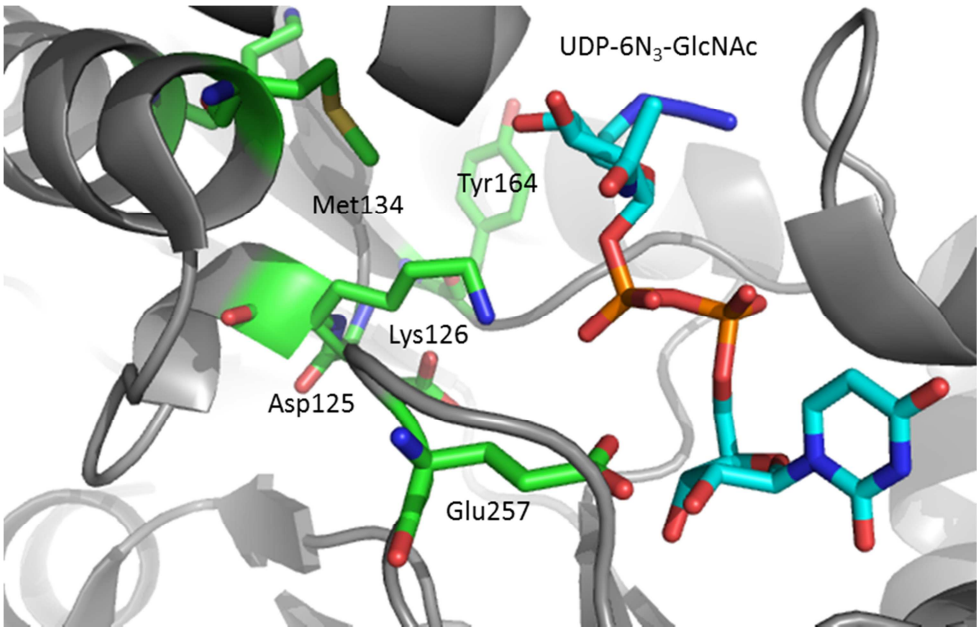

Fig. 4.8. Active site of the capsular polysaccharide synthesizing protein CapE with UDP-$6N_3$-GlcNAc occupying the substrate-binding site. Active site residues are labelled.

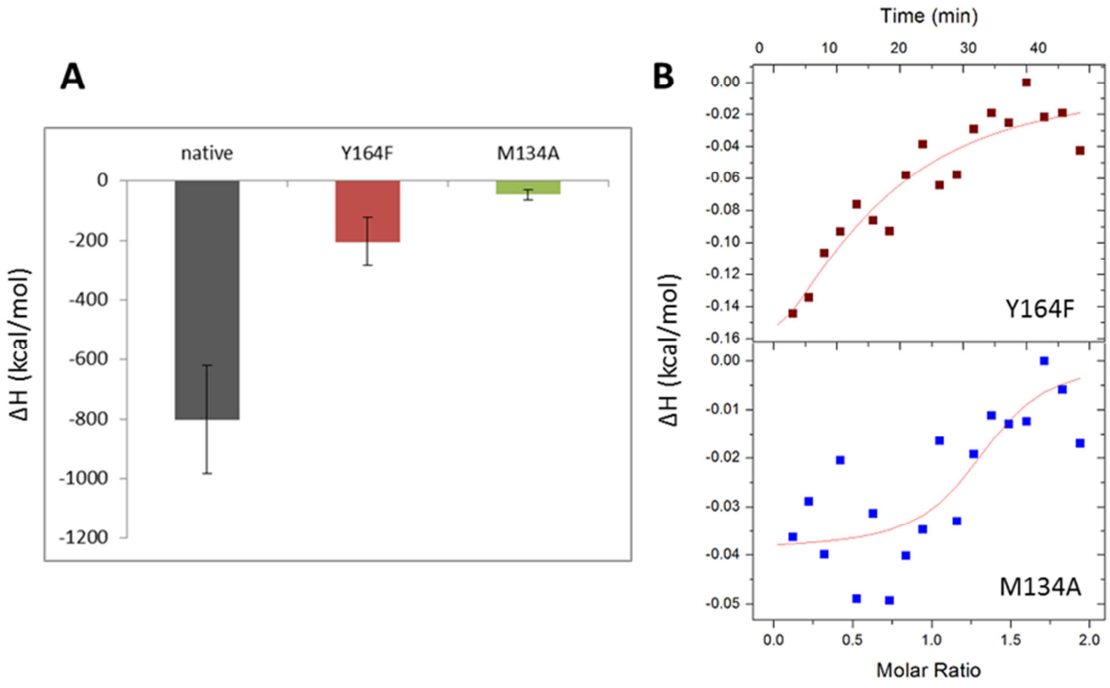

Fig 4.9. Binding comparisons between native ***Ab*-WbjB** and two mutants, M134A and Y164F. (A) Average enthalpies of binding for each protein as measured by ITC, with error bars shown. Mutants (20 µM) were screened in Buffer A with 1 mM NADP and 1 mM UDP-GlcNAc (B) Best fit curves for each of the mutants.

binding of NADP between native ***Ab*-WbjB** and the Y164F mutant using DSF might shed light on this possibility.

4.5 Crystallising complexes of *Ab*-WbjB

As preparations of ***Ab*-WbjB** have previously crystallised with NADP bound, the next aim was to determine the effect of UDP-GlcNAc on crystallisation of any complex. Dr. Bhumika Shah had found that crystals of ***Ab*-WbjB** with NADP tend to grow best under acidic conditions (pH 5.6) [16]. However, my DSF screens had suggested higher pH to be favourable for stability. Thus, crystallisation trays were set up at both pH 5.6 and 8.0. Fig. 4.10 shows the general layout of one tray.

Each screen was set up with ***Ab*-WbjB** protein samples, and a variable amount of NADP and UDP-GlcNAc. The first row of each tray contained only NADP (1 to 2 mM), whereas the last row contained only UDP-GlcNAc (1 to 2 mM). The two middle rows contained both compounds, with row B containing a 1:2 ratio of UDP-GlcNAc (0.3 to 0.7 mM) to NADP (0.7 to 1.3 mM), and row C at a 2:1 ratio. The pH 5.6 tray only grew crystals in wells containing NADP, with all other wells showing heavy protein precipitate. This growth happened immediately after the trays were laid down, and protein conditions did not change after this. Fig. 4.11 shows crystals that grew in pH 8.0 wells containing NADP and UDP-GlcNAc after one month. These crystals were found in wells containing 1.2 to 2 mM NADP, 0.7 to 1.2 mM NADP and 0.3 to 0.6 mM UDP-GlcNAc, and one well containing 0.3 mM NADP and 0.7 mM UDP-GlcNAc (Fig. 4.10). My previous ITC results show that UDP-GlcNAc will not bind to ***Ab*-WbjB** without the presence of excess NADP. This is supported by the trend of crystal growth seen in Fig. 4.11. Crystals were all in the shape of octahedrons, but varied in size and abundance.

Before pursuing diffraction acquisition, sample crystals were taken from wells of interest (pH 8.0, 1.1 mM NADP, 0.55 mM UDP-GlcNAc) and tested for the presence of protein. This was done in order to rule out that the crystals observed contained only salt. Fig. 4.12 shows an SDS-PAGE gel from re-solubilising the crystals in mother liquor (30 µl) [86]. Samples were washed three times with the same amount of mother liquor in order to remove any protein in solution. The final washed sample was compared against ***Ab*-WbjB** protein samples from the same purification. Excitingly, the band observed in Fig. 4.12 clearly confirmed that ***Ab*-**

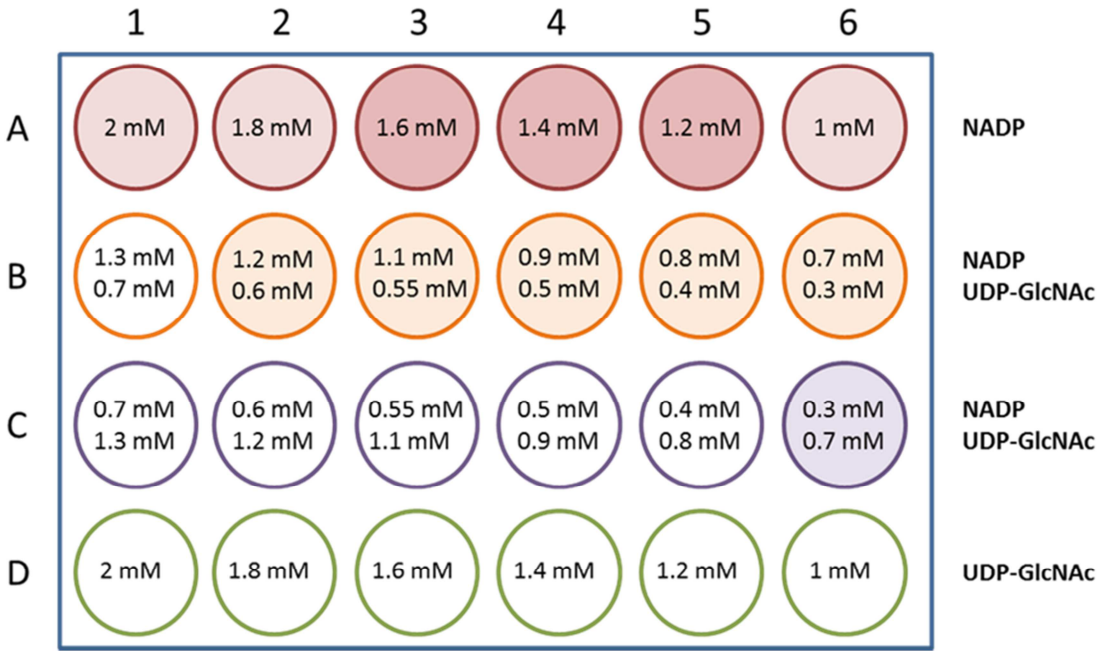

Fig. 4.10. Lay out of 24-well hanging-drop plate containing ***Ab*-WbjB** in Buffer A. Two plates were set up at pH 5.6 and 8.0. Concentrations of NADP and UDP-GlcNAc are displayed in each well. Wells that are shaded grew crystals, with darker shades having displayed crystals in both the pH 5.6 and pH 8.0 plates.

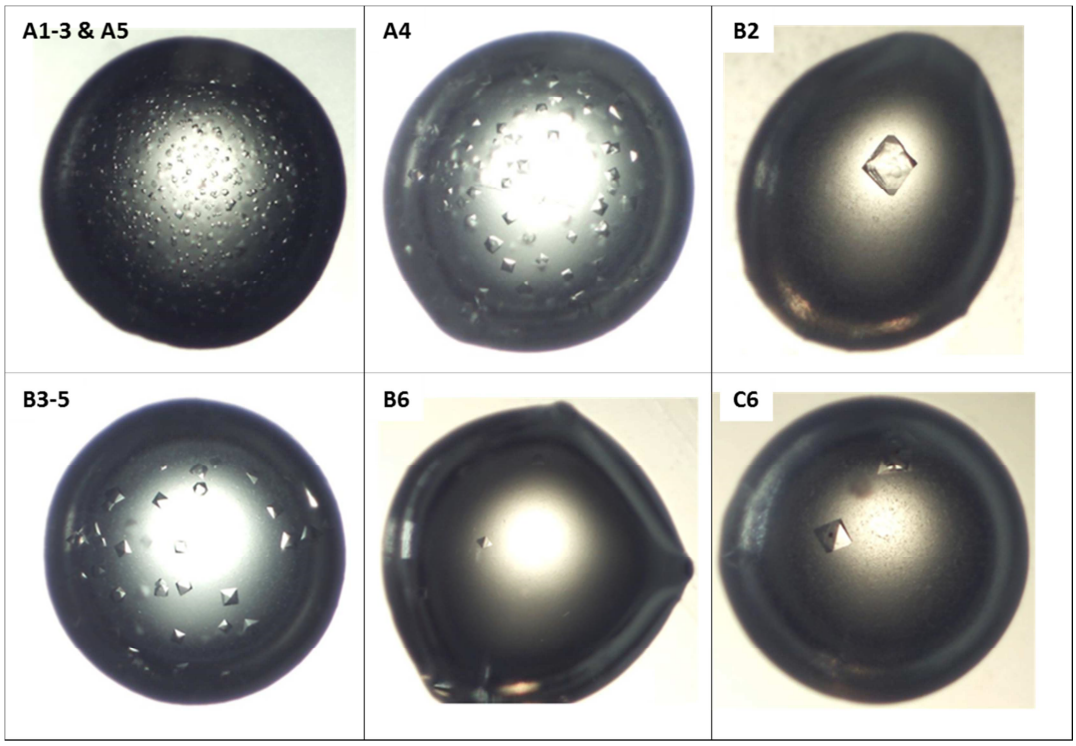

Fig. 4.11. Different crystal sizes seen for pH 8.0 plate. Crystals have been sorted as dictated by Fig. 4.10.

WbjB was present in the crystals sampled. For this reason, the harvested crystals were taken to the Australian Synchrotron (Melbourne).

All crystals were transported, mounted, and diffraction data collected by Dr. Shah. All crystals tested were a good size (0.1 to 0.5 mm), shape, and contained protein. Out of twenty crystals tested, the best diffraction was obtained for crystal # 2 from well C6 (0.3 mM NADP, 0.7 mM UDP-GlcNAc, pH 8.0) yielding a resolution of 5.4 Å and was found in a cubic lattice (1.2×10^7 Å^3, Table 4.1) [71]. A diffraction pattern for this crystal can be seen in Fig. 4.13 in comparison with a previous diffraction pattern of ***Ab*-WbjB** in complex with NADP (2.65 Å) [16]. The diffraction pattern on the left indicates that resolution for this crystal was very low (>5 Å). Unfortunately, this resolution was too low for any structure solving, even by the method of molecular replacement [70]. The generally low resolution was due to the disorder in the crystals, and possibly degradation due to X-ray damage (crystal was exposed for 3 min) [74, 75]. Only 180 images were taken before radiation damage was observed.

In order to obtain a crystal structure of ***Ab*-WbjB** with NADP and UDP-GlcNAc occupying the cofactor-binding and substrate-binding domain, further optimisation of crystallisation conditions will need to be carried out.

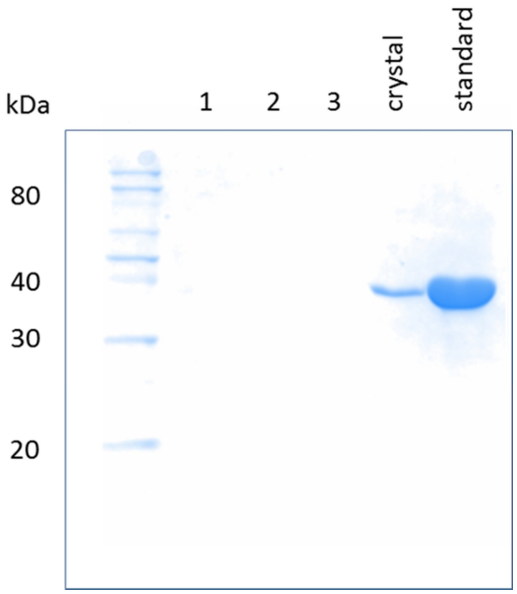

Fig. 4.12. SDS-PAGE gel of samples derived from re-solubilised protein crystals. Excess crystals from well B3 (pH 8.0, 1.1 mM NADP, 0.55 mM UDP-GlcNAc) were re-solubilised in mother liquor and run by SDS-PAGE next to a fresh sample of purified ***Ab*-WbjB** (standard). Numbers 1, 2, and 3 represent washes of crystals with fresh mother liquor.

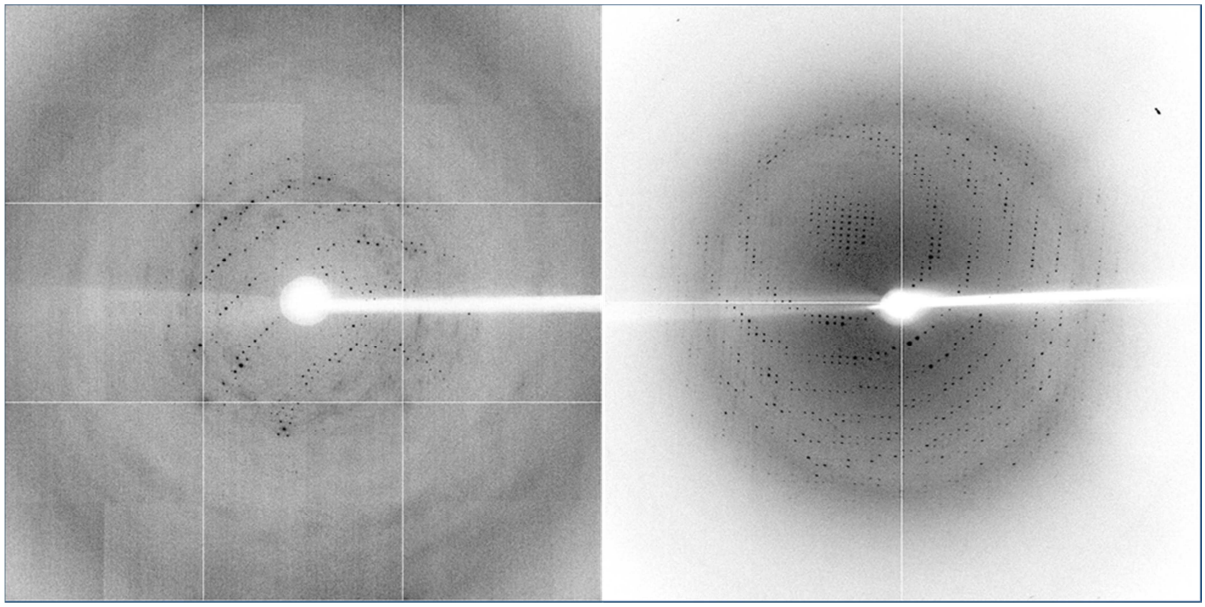

Fig. 4.13. Diffraction patterns from ***Ab*-WbjB**. On the left is the diffraction pattern from ***Ab*-WbjB** crystallised during this experiment (pH 8.0, well C6, crystal #2). On the right is the diffraction pattern from crystals of ***Ab*-WbjB** previously grown by Dr. Shah (pH 5.6, <3 Å).

Table 4.1. Crystal data collection from well C6, crystal number 2, pH 8.0

wavelength (Å)	0.9537
images	180
space group	$F4_132$
a, b, c (Å)	227.4, 227.4, 227.4
α, β, γ (˚)	90, 90, 90
resolution (Å)	46.41 – 5.46 (6.11 – 5.46)
number of unique reflections	1909 (514)
completeness (%)	99.8 (100.0)
multiplicity	19.1 (20.1)
mean $I/\sigma(I)$	25.8 (3.3)

Chapter 5: *Acinetobacter baumannii* gene knockout

5.1 Gene knockout construction in non-competent Gram-negative bacteria

Disruption of a target gene is essential for revealing the biological functions of the gene and its product in an organism. This can be done through the process of gene knockouts, where a gene is either silenced or replaced in the organism's genome [87]. Competent bacteria can be mutated simply by introducing a PCR product that will become integrated through homologous recombination [88]. However, the process becomes more difficult when using non-competent Gram-negative bacteria such as *A. baumannii*. Such Gram-negative bacteria are frequently mutated by a plasmid-based method, in which plasmid DNA is introduced into the cell by bacterial conjugation, and allelic marker exchange is then carried out by homologous recombination between the chromosomal DNA and the introduced allele on a gene replacement plasmid [89-91]. In this case it is essential to obtain a double crossover mutant which can be detected through a counter-selection marker such as *sacB* [92], or antibiotic resistance.

One goal of my project was to achieve a double crossover knockout in *A. baumannii* targeting the gene *fnlA* which encodes for ***Ab*-WbjB**. As outlined in Chapter 1, in *A. baumannii* (community strain D1279779), *fnlA* is part of a polysaccharide synthesis cluster (Fig. 1.1) [12]. It is still unknown whether this specific pathway in ***Ab*-WbjB** functions to produce sugars bound for the bacterial capsule of *A. baumannii* [51], or if they serve another purpose.

In a clinical strain of *A. baumannii* (MDR-TJ), a similar nucleotide sugar synthesis pathway has been identified with high sequence similarity of the component proteins (81 to 58 % identity) [34]. The pathway in MDR-TJ is, however, missing the gene (*gdr*) necessary to transport any resulting UDP-D-Qui*p*NAc to the capsule. Nevertheless, there does appear to be remnants of *gdr*. This example shows that there are great differences even in bacteria of the same species.

5.2 Design and assembly of *flnA* knockout vector

In order to eventually probe the biological manifestation of the enzyme ***Ab*-WbjB** in *A. baumannii* cells, a specific knockout of *fnlA* was planned in *A. baumannii*. This approach was decided upon as it would help to determine the exact role of ***Ab*-WbjB** in the bacteria,

whereas knocking out the entire WbjBCD pathway may result in changes unassociated with the protein. The general method used for the gene knockout procedure was adapted from work by Choi and Schweizer [24], in which a gene knockout was constructed in *Pseudomonas aeruginosa* using a suicide vector containing genes flanking the desired deletion, as well as an antibiotic resistance gene. The vector was then transferred to *P. aeruginosa* using a rapid transformation procedure and recombined into the bacterial chromosome. In order to screen for double crossover events in which the whole construct has replaced the target gene, the bacteria were subsequently resolved by gentamycin counter-selection.

To adapt this procedure for my gene of interest in *A. baumannii*, primers for the *fnlA* knockout vector insert were designed to amplify regions upstream and downstream from *fnlA*, and as well incorporate kanamycin resistance (Fig. 5.1). Amplification of the regions flanked by each primer would result in three PCR products (Up_ *fnlA*, Dn_ *fnlA*, and Km). The Kanamycin resistance gene was added to act as an endpoint selection marker, inserted backwards in order to prevent amplification of downstream genes. *Pst*I and *Bam*HI restriction sites were also engineered into the Up_ *fnlA* and Dn_ *fnlA* sections (Fig. 5.1) to provide sticky ends for the final ligation step into the suicide vector (Section 2.2.3).

To make the *fnlA* knockout vector insert, two PCR cycles were required. The first PCR cycle (section 2.2.3) was designed to amplify Up_ *fnlA*, Dn_ *fnlA*, and Km sections of the insert seen in Fig 5.1. Up primers (0.8 µM) and their matching Dn primers (0.8 µM) were combined with D1279779 DNA (50 ng) to form the two constructs, Up_ *fnlA* and Dn_ *fnlA*. Primers Up_R and Dn_F (0.2 µM) were combined with Kanamycin (Km) DNA (14.5 ng) to form the third construct. As amplification of the kanamycin gene was not first successful, likely due to self-annealing sections of the primers, a previously amplified segment was obtained from Karl Hassan (Macquarie University). Up_ *fnlA* constructs were 1.2 kb in size, Dn_ *fnlA* constructs 1.1 kb, and Km constructs 600 bp, which can be seen in Fig. 5.2.

With all necessary constructs to hand, a second PCR cycle was performed to form the required vector insert (*fnlA*'Km). All constructs were combined in one overlap extension reaction, allowed to anneal for 5 min, and with the addition of Up_F and Dn_R primers (1 µl each), amplified for another hour. Annealing was able to occur as each construct had been designed with overlapping DNA sequences, allowing for easy ligation. The resulting vector

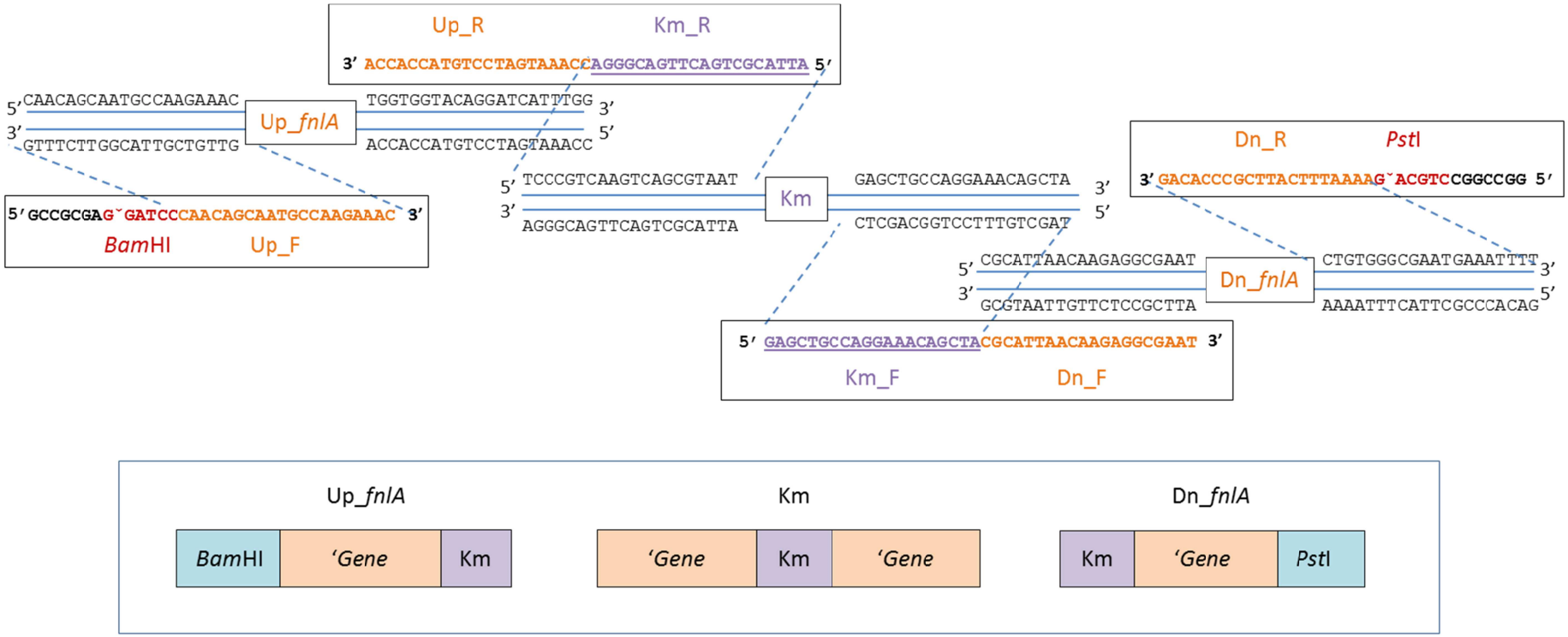

Fig. 5.1. Primer design for *fnlA* gene knockout in *A. baumannii*. The double-stranded sequences for the upstream and downstream regions from *fnlA* are shown between primers designed to amplify regions of these genes, along with the kanamycin gene in PCR cycle 1. Km primer sequences are in purple, *fnlA* primer sequences in orange, and enzyme restriction sites in red. Once amplification of these genes has occurred, there will be three constructs (Up_*fnlA*, Dn_*fnlA*, and Km) which can be ligated together in PCR cycle 2 due to overlapping regions of DNA sequence.

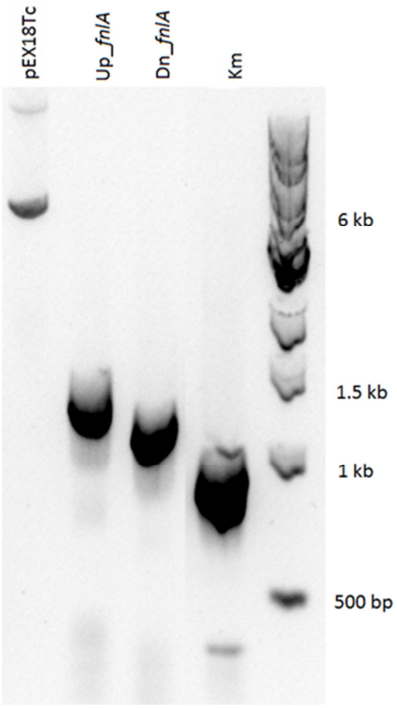

Fig. 5.2. DNA products shown on a 1.2 % agarose gel. On the left is plasmid pEX18Tc at approximately 6 kb. In the middle are PCR products of the upstream (1.2 kb) and downstream (1.1 kb) constructs. The Kanamycin construct (Km) on the right is approximately 600 bp, gift of Karl Hassan.

insert, *fnlA*'Km (3 kb), will be suitable to replace the *fnlA* gene using homologous recombination within *A. baumannii*.

The suicide vector, pEX18Tc (seen in Fig. 5.3) was chosen for delivery of *fnlA*'Km to the host, and contains a tetracycline resistance gene (*tet*) for antibiotic selection, a lvansucrase-encoding gene (*SacB*) allowing it to grow on sucrose media [93], and a *LacZ* gene for X-gal selection [94]. *Pst*I and *Bam*HI were chosen as restriction enzymes due to their buffer compatibility and excision site positions in suicide vector pEX18Tc. Both *fnlA*'Km and pEX18Tc were separately digested with PstI and BamHI enzymes for 3 h, in order to create sticky ends and allow for ligation of *fnlA*'Km into pEX18Tc. As seen in Fig. 5.4, the plasmid became linearised when digested, resulting in a product that appeared to be larger. This was due to the supercoiled plasmid straightening out and taking more time to run through the agarose gel. The digestion of *fnlA*'Km resulted in a similar sized product, as only a few base pairs were removed from either end of the construct.

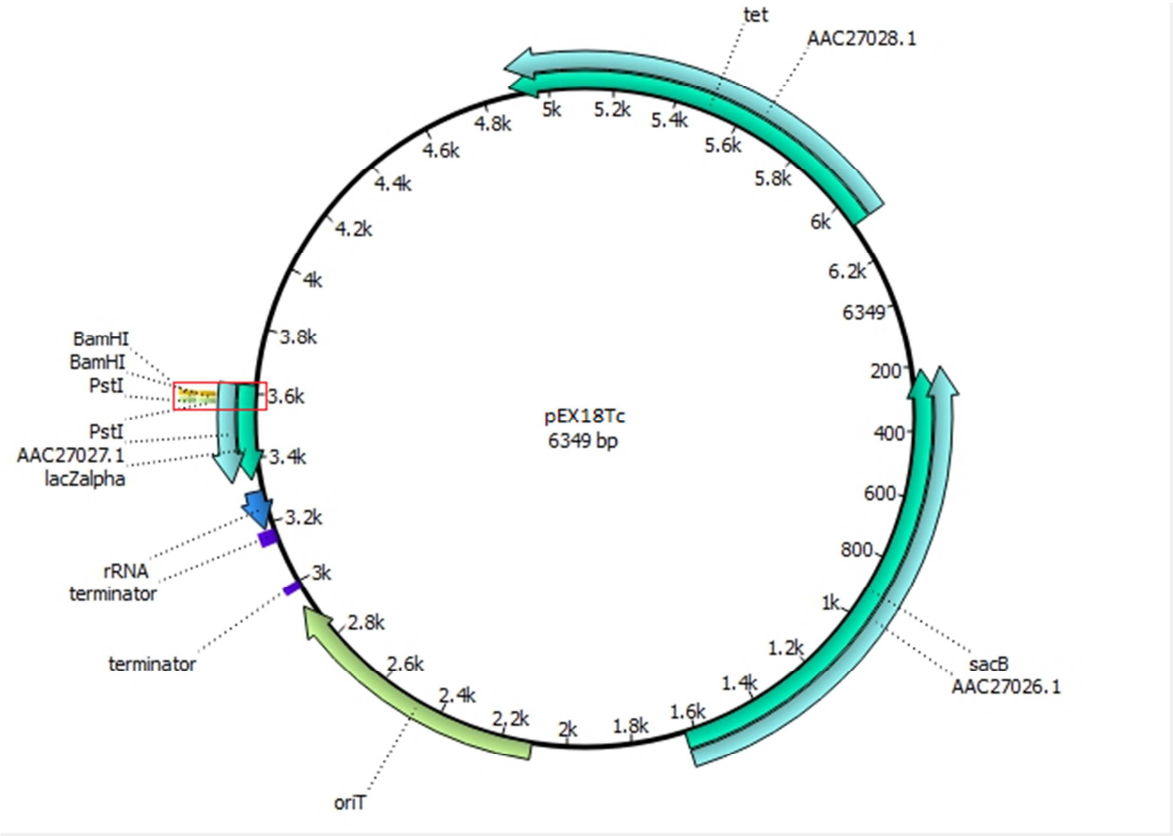

Fig 5.3. Map of pEX18Tc plasmid [90]. Restriction sites have been marked for *Bam*HI and *Pst*I, which were used in primer design. The excised region is approximately 18 bp in size and interrupts the *LacZ* gene. *sacB* and *tet* genes are alternative selection markers for the plasmid.

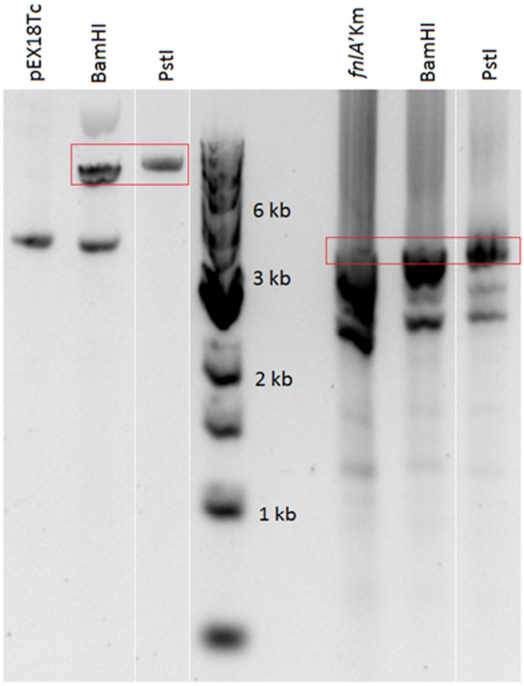

Fig. 5.4. DNA products shown on a 1.2 % agarose gel. On the left is the supercoiled pEX18Tc plasmid which was cut with BamHI and PstI enzymes, resulting in a linearised plasmid. On the right is the unpurified PCR product for the vector insert, *fnlA*'Km. The main band at 3 kb is the insert, with other bands below representing unsuccessfully ligated constructs (Up_ *fnlA*, Dn_ *fnlA*, and Km). *fnlA*'Km was also cut with BamHI and PstI resulting in products of the same size.

Chapter 6: Conclusions and future directions

6.1 NADP plays an important role in stabilising *Ab*-WbjB

The Gram-negative bacillus *A. baumannii* is an emerging multidrug-resistant, opportunistic pathogen. Increasing resistance to antibiotics is thought to be due in part to highly variable genomic islands and lateral gene transfer. *fnlA*, found in a genomic island of the D1279779 strain of *A. baumannii*, encodes for the protein ***Ab*-WbjB**, an extended short-chain dehydrogenase/reductase (SDR). SDRs are commonly known to display a fully conserved Rossmann-fold where the cofactor, NADPH, binds tightly [77, 78]. The substrates for these enzymes range from alcohols and sugars, to steroids, xenobiotics, and aromatic compounds [43]. They are on a whole a well characterised family of enzymes [40, 77, 95], and although ***Ab*-WbjB** is similar in structure to other members of the SDR family, little is known about its function in *A. baumannii*.

***Ab*-WbjB** tightly binds a cofactor, NADPH, which undergoes different redox state changes during the reaction cycle. My research reveals variability in the quaternary structure of ***Ab*-WbjB** in presence and absence of reducing agents. In the presence of reducing agents such as TCEP and DTT, this enzyme oligomerises as a hexamer. However under non-reducing conditions, ***Ab*-WbjB** takes the form of a dimer. Thus, I have successfully demonstrated that buffer conditions can upset the redox state of NADP, and it is likely that addition of a reductant alters the cofactor environment to change the oligometric state of the protein.

In addition, DSF experiments tested the role of NADP with regards to overall stability of ***Ab*-WbjB** and its effects on substrate binding. This work demonstrated increase in protein stability when excess cofactor is added to buffers. Additionally, my ITC experiments indicated that the presence of NADP is essential for substrate binding. It has been shown in epimerases that the binding of UDP to the nucleotide-diphosphate domain enhances reactivity of NAD+, suggesting cooperative behaviour between the UDP-binding domain and the central catalytic domain [77]. My research indicates similar behaviours in NADP dependent ***Ab*-WbjB**, with a lack of cofactor adversely affecting the substrate binding event.

6.2 UDP-GlcNAc, a putative substrate for *Ab*-WbjB

***Ab*-WbjB** shows a high degree of structural similarity with other members of the SDR family: CapE, a capsular polysaccharide-synthesising enzyme from *Staphylococcus aureus* [48] and

FlaA1, a flagella glycosylation protein found in *Helicobacter pylori* [49]. CapE has been shown to bind UDP-6N3-GlcNAc, whereas the structure of FlaA1 was solved with UDP-GlcNAc occupying the active site [50].

In the crystal structure of ***Ab*-WbjB**, NADP is found to be tightly bound to the cofactor-binding site [16]. Although this site in SDRs is well understood and characterised, there is less of a consensus when it comes to substrate binding. For this reason, the substrate-binding site was extensively examined using ITC. My work has identified UDP-GlcNAc as a probable substrate for ***Ab*-WbjB**. The analysis on several different structural iterations of UDP-GlcNAc (GlcNAc, UDP-Glc, and glucosamine) showed that the dinucleotide portion of the sugar is absolutely necessary for binding to ***Ab*-WbjB**. It is well documented in the literature that the binding of UDP sugars only occurs at the dinucleotide portion, facilitating the rotation of the sugar, and allowing modification by the enzyme [77, 83, 84].

Further studies on UDP-GlcNAc are required to pursue its interaction with ***Ab*-WbjB**. This could be achieved through the use of capillary electrophoresis [29, 48, 96] or surface plasmon resonance [97, 98]. Capillary electrophoresis has previously been employed for both CapE and FlaA1 and showed modification of substrate by the protein. Surface plasmon resonance is a complementary technique to ITC and can show precise binding of compounds to a protein.

Co-crystallisation attempts of ***Ab*-WbjB** with bound UDP-GlcNAc and NADP successfully produced crystals containing both compounds at pH 8.0, however, in order to obtain a good quality diffraction data set, further optimisation is required. Techniques such as microseeding and changing pH, temperature, and salt concentrations can be applied for this purpose. In addition, ***Ab*-WbjB** mutants obtained during my research (M134A and Y164F) are also a good starting point for crystallisation, as inactivity of the active site may facilitate well-ordered crystals. When crystallisation and subsequent X-ray scattering is successful, structural interactions with the substrate could be visualised and better understood.

6.3 Inferences relating to active site binding of *Ab*-WbjB

The substrate-binding site of SDRs shows more variation than the cofactor-binding site, but generally consists of the residue triad Ser, Tyr, and Lys [40, 45]. For extended SDRs, the active site motif is generally seen as YxxxK, however, this sequence motif is not fully

conserved in ***Ab*-WbjB** [77]. As with CapE, it displays a catalytic triad composed of Met instead of Tyr seen in most other SDRs (MxxxK) [51].

By changing residues close in proximity to the substrate-binding site, I was able to observe changes in binding efficiency for ***Ab*-WbjB**. Two mutants, M134A and Y164F, were tested for this purpose. Met134 proved to be absolutely necessary for substrate binding, whereas Tyr164 affected binding capability to a lesser extent. In CapE, it is speculated that the presence of Met in the binding pocket is tied to a novel latch structure [48]. This latch is thought to regulate the access of substrate to the binding pocket as it is positioned at the entrance to this site. Therefore, my mutation of M134A may have disabled the latch and compromised substrate binding capabilities. The role of Tyr164 is still unknown, and further studies are required to determine its role in active site chemistry.

It is likely that Met134 and Tyr164 mutations compromised the binding of NADP to ***Ab*-WbjB**, as the residues are close in proximity to the cofactor-binding site, and this in turn impaired binding of the substrate. In order to verify this hypothesis, further fluorescent binding assays on these mutants would be beneficial.

6.4 Successful construction of a vector insert for *fnlA* gene knockout

Two closest homologues of ***Ab*-WbjB,** CapE and FlaA1, are predicted to serve different functions. While CapE from *S. aureus* is a capsular polysaccharide-synthesising enzyme, FlaA1 is thought to be involved in glycosylation of flagella proteins. It is therefore unknown whether the pathway in which ***Ab*-WbjB** plays a role, produces sugars bound for the bacterial capsule of *A. baumannii*, or if they serve another purpose. Thus in the absence of any consensus to the function of nucleotide sugars produced by ***Ab*-WbjB**, we planned a gene knockout study to determine its effect on *A. baumannii*.

I have successfully prepared a 3 kb suicide vector insert, *fnlA*'Km. Future work to complete gene knockout preparation is shown in Fig. 6.1. It involves ligation of the *fnlA*'Km construct into the suicide vector (pEX18Tc) followed by introduction into *A. baumannii*. Positive knockouts could then be screened by sucrose or Kanamycin counterselection, and observed in order to view changes in bacterial function or appearance. This could be achieved through use of a Biolog plate, which would allow the native bacteria to be compared to the knockouts under a variety of growth conditions, including the screening of antibiotic

resistance [99-101]. Another way to observe this change would be through the introduction of both *A. baumannii* strains to a host. In this way the host fitness could be monitored in response to each pathogen. Analysis of changes to surface glycans could be achieved through the use of Mass Spectrometry and silver staining techniques [102, 103]. This makes for an exciting project that would aid in understanding the role that *fnlA* plays in bacterial virulence, drug resistance or host adaptation.

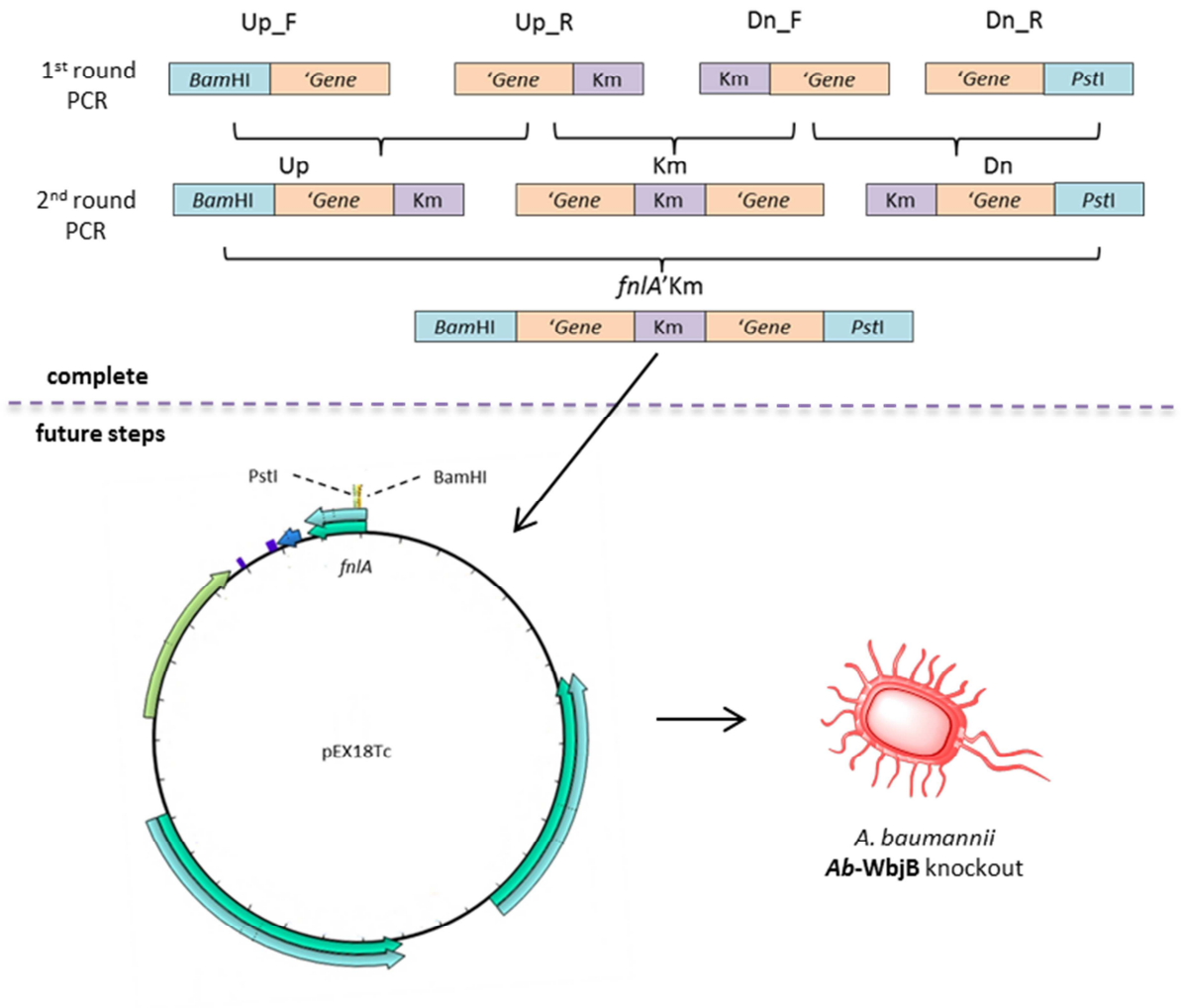

Fig. 6.1. *Ab*-WbjB knockout procedure in *A. baumannii*. Steps above the dotted line have been completed in this research. All steps below the line still need to be carried out.

6.5 Concluding remarks

The structure of ***Ab*-WbjB**, solved at Macquarie University, has established a link to a sugar operon and polysaccharide biosynthesis cluster in *A. baumannii*. My work in this direction has reinforced the fact that ***Ab*-WbjB** plays a crucial role in polysaccharide biosynthesis. Additionally, the analysis of the active site chemistry and mutants has opened up a number of avenues for future investigations.

References

[1] Howard A, O'Donoghue M, Feeney A, Sleator RD. *Acinetobacter baumannii*: an emerging opportunistic pathogen. Virulence. 2012;3:243-50.

[2] Montefour K, Frieden J, Hurst S, Helmich C, Headley D, Martin M, et al. *Acinetobacter baumannii*: an emerging multidrug-resistant pathogen in critical care. Crit Care Nurse. 2008;28:15-25; quiz 6.

[3] Centers for Disease C, Prevention. *Acinetobacter baumannii* infections among patients at military medical facilities treating injured U.S. service members, 2002-2004. MMWR Morb Mortal Wkly Rep. 2004;53:1063-6.

[4] Chen MZ, Hsueh PR, Lee LN, Yu CJ, Yang PC, Luh KT. Severe community-acquired pneumonia due to *Acinetobacter baumannii*. Chest. 2001;120:1072-7.

[5] Poirel L, Bonnin RA, Nordmann P. Genetic basis of antibiotic resistance in pathogenic *Acinetobacter* species. IUBMB Life. 2011;63:1061-7.

[6] Tomaras AP, Dorsey CW, Edelmann RE, Actis LA. Attachment to and biofilm formation on abiotic surfaces by *Acinetobacter baumannii*: involvement of a novel chaperone-usher pili assembly system. Microbiology. 2003;149:3473-84.

[7] Bayuga S, Zeana C, Sahni J, Della-Latta P, el-Sadr W, Larson E. Prevalence and antimicrobial patterns of *Acinetobacter baumannii* on hands and nares of hospital personnel and patients: the iceberg phenomenon again. Heart Lung. 2002;31:382-90.

[8] Visca P, Seifert H, Towner KJ. *Acinetobacter* infection--an emerging threat to human health. IUBMB Life. 2011;63:1048-54.

[9] Higgins PG, Dammhayn C, Hackel M, Seifert H. Global spread of carbapenem-resistant *Acinetobacter baumannii*. J Antimicrob Chemother. 2010;65:233-8.

[10] Rodriguez-Martinez JM, Nordmann P, Ronco E, Poirel L. Extended-spectrum cephalosporinase in *Acinetobacter baumannii*. Antimicrob Agents Chemother. 2010;54:3484-8.

[11] Poirel L, Nordmann P. Carbapenem resistance in *Acinetobacter baumannii*: mechanisms and epidemiology. Clin Microbiol Infect. 2006;12:826-36.

[12] Farrugia DN, Elbourne LD, Hassan KA, Eijkelkamp BA, Tetu SG, Brown MH, et al. The complete genome and phenome of a community-acquired *Acinetobacter baumannii*. PLoS One. 2013;8:e58628.

[13] Peleg AY, Seifert H, Paterson DL. *Acinetobacter baumannii*: emergence of a successful pathogen. Clin Microbiol Rev. 2008;21:538-82.

[14] Post V, White PA, Hall RM. Evolution of AbaR-type genomic resistance islands in multiply antibiotic-resistant *Acinetobacter baumannii*. J Antimicrob Chemother. 2010;65:1162-70.

[15] Towner KJ, Evans B, Villa L, Levi K, Hamouda A, Amyes SG, et al. Distribution of intrinsic plasmid replicase genes and their association with carbapenem-hydrolyzing class D beta-lactamase genes in European clinical isolates of *Acinetobacter baumannii*. Antimicrob Agents Chemother. 2011;55:2154-9.

[16] Shah BS. Genomic island components within Australian *A. baumannii* strains: sequences and protein structures. Sydney, NSW, Australia: Macquarie University; 2013.

[17] Sullivan JT, Trzebiatowski JR, Cruickshank RW, Gouzy J, Brown SD, Elliot RM, et al. Comparative sequence analysis of the symbiosis island of Mesorhizobium loti strain R7A. J Bacteriol. 2002;184:3086-95.

[18] Gaillard M, Vallaeys T, Vorholter FJ, Minoia M, Werlen C, Sentchilo V, et al. The clc element of Pseudomonas sp. strain B13, a genomic island with various catabolic properties. J Bacteriol. 2006;188:1999-2013.
[19] Larbig KD, Christmann A, Johann A, Klockgether J, Hartsch T, Merkl R, et al. Gene islands integrated into tRNA(Gly) genes confer genome diversity on a Pseudomonas aeruginosa clone. J Bacteriol. 2002;184:6665-80.
[20] Fournier PE, Vallenet D, Barbe V, Audic S, Ogata H, Poirel L, et al. Comparative genomics of multidrug resistance in *Acinetobacter baumannii*. PLoS Genet. 2006;2:e7.
[21] Tomaras AP, Flagler MJ, Dorsey CW, Gaddy JA, Actis LA. Characterization of a two-component regulatory system from *Acinetobacter baumannii* that controls biofilm formation and cellular morphology. Microbiology. 2008;154:3398-409.
[22] Loehfelm TW, Luke NR, Campagnari AA. Identification and characterization of an *Acinetobacter baumannii* biofilm-associated protein. J Bacteriol. 2008;190:1036-44.
[23] Gaddy JA, Tomaras AP, Actis LA. The *Acinetobacter baumannii* 19606 OmpA protein plays a role in biofilm formation on abiotic surfaces and in the interaction of this pathogen with eukaryotic cells. Infect Immun. 2009;77:3150-60.
[24] Choi KH, Schweizer HP. An improved method for rapid generation of unmarked *Pseudomonas aeruginosa* deletion mutants. BMC Microbiol. 2005;5:30.
[25] Barbe V, Vallenet D, Fonknechten N, Kreimeyer A, Oztas S, Labarre L, et al. Unique features revealed by the genome sequence of *Acinetobacter* sp. ADP1, a versatile and naturally transformation competent bacterium. Nucleic Acids Res. 2004;32:5766-79.
[26] Robinson A, Guilfoyle AP, Sureshan V, Howell M, Harrop SJ, Boucher Y, et al. Structural genomics of the bacterial mobile metagenome: an overview. Methods Mol Biol. 2008;426:589-95.
[27] Sureshan V, Deshpande CN, Boucher Y, Koenig JE, Midwest Center for Structural G, Stokes HW, et al. Integron gene cassettes: a repository of novel protein folds with distinct interaction sites. PLoS One. 2013;8:e52934.
[28] Deshpande CN, Harrop SJ, Boucher Y, Hassan KA, Di Leo R, Xu X, et al. Crystal structure of an integron gene cassette-associated protein from Vibrio cholerae identifies a cationic drug-binding module. PLoS One. 2011;6:e16934.
[29] Mulrooney EF, Poon KK, McNally DJ, Brisson JR, Lam JS. Biosynthesis of UDP-N-acetyl-L-fucosamine, a precursor to the biosynthesis of lipopolysaccharide in *Pseudomonas aeruginosa* serotype O11. J Biol Chem. 2005;280:19535-42.
[30] Adams MD, Goglin K, Molyneaux N, Hujer KM, Lavender H, Jamison JJ, et al. Comparative genome sequence analysis of multidrug-resistant *Acinetobacter baumannii*. J Bacteriol. 2008;190:8053-64.
[31] Vallenet D, Nordmann P, Barbe V, Poirel L, Mangenot S, Bataille E, et al. Comparative analysis of *Acinetobacters*: three genomes for three lifestyles. PLoS One. 2008;3:e1805.
[32] Iacono M, Villa L, Fortini D, Bordoni R, Imperi F, Bonnal RJ, et al. Whole-genome pyrosequencing of an epidemic multidrug-resistant *Acinetobacter baumannii* strain belonging to the European clone II group. Antimicrob Agents Chemother. 2008;52:2616-25.
[33] Smith MG, Gianoulis TA, Pukatzki S, Mekalanos JJ, Ornston LN, Gerstein M, et al. New insights into *Acinetobacter baumannii* pathogenesis revealed by high-density pyrosequencing and transposon mutagenesis. Genes Dev. 2007;21:601-14.
[34] Kenyon JJ, Hall RM. Variation in the complex carbohydrate biosynthesis loci of *Acinetobacter baumannii* genomes. PLoS One. 2013;8:e62160.
[35] Whitfield C. Biosynthesis and assembly of capsular polysaccharides in *Escherichia coli*. Annu Rev Biochem. 2006;75:39-68.
[36] Needham BD, Trent MS. Fortifying the barrier: the impact of lipid A remodelling on bacterial pathogenesis. Nat Rev Microbiol. 2013;11:467-81.

[37] Raetz CR, Reynolds CM, Trent MS, Bishop RE. Lipid A modification systems in Gram-negative bacteria. Annu Rev Biochem. 2007;76:295-329.
[38] Guo L, Lim KB, Poduje CM, Daniel M, Gunn JS, Hackett M, et al. Lipid A acylation and bacterial resistance against vertebrate antimicrobial peptides. Cell. 1998;95:189-98.
[39] Boulnois GJ, Jann K. Bacterial polysaccharide capsule synthesis, export and evolution of structural diversity. Mol Microbiol. 1989;3:1819-23.
[40] Jornvall H, Persson B, Krook M, Atrian S, Gonzalez-Duarte R, Jeffery J, et al. Short-chain dehydrogenases/reductases (SDR). Biochemistry. 1995;34:6003-13.
[41] Ghosh D, Sawicki M, Pletnev V, Erman M, Ohno S, Nakajin S, et al. Porcine carbonyl reductase. structural basis for a functional monomer in short chain dehydrogenases/reductases. J Biol Chem. 2001;276:18457-63.
[42] Krook M, Ghosh D, Stromberg R, Carlquist M, Jornvall H. Carboxyethyllysine in a protein: native carbonyl reductase/NADP(+)-dependent prostaglandin dehydrogenase. Proc Natl Acad Sci U S A. 1993;90:502-6.
[43] Kallberg Y, Oppermann U, Jornvall H, Persson B. Short-chain dehydrogenase/reductase (SDR) relationships: a large family with eight clusters common to human, animal, and plant genomes. Protein Sci. 2002;11:636-41.
[44] Lesk AM. NAD-binding domains of dehydrogenases. Curr Opin Struct Biol. 1995;5:775-83.
[45] Oppermann UC, Filling C, Jornvall H. Forms and functions of human SDR enzymes. Chem Biol Interact. 2001;130-132:699-705.
[46] Rossmann MG, Moras D, Olsen KW. Chemical and biological evolution of nucleotide-binding protein. Nature. 1974;250:194-9.
[47] Holm L, Rosenstrom P. Dali server: conservation mapping in 3D. Nucleic Acids Res. 2010;38:W545-9.
[48] Miyafusa T, Caaveiro JM, Tanaka Y, Tanner ME, Tsumoto K. Crystal structure of the capsular polysaccharide synthesizing protein CapE of *Staphylococcus aureus*. Biosci Rep. 2013;33.
[49] Creuzenet C, Schur MJ, Li J, Wakarchuk WW, Lam JS. FlaA1, a new bifunctional UDP-GlcNAc C6 Dehydratase/ C4 reductase from *Helicobacter pylori*. J Biol Chem. 2000;275:34873-80.
[50] Ishiyama N, Creuzenet C, Miller WL, Demendi M, Anderson EM, Harauz G, et al. Structural studies of FlaA1 from *Helicobacter pylori* reveal the mechanism for inverting 4,6-dehydratase activity. J Biol Chem. 2006;281:24489-95.
[51] Miyafusa T, Caaveiro JM, Tanaka Y, Tsumoto K. Dynamic elements govern the catalytic activity of CapE, a capsular polysaccharide-synthesizing enzyme from *Staphylococcus aureus*. FEBS Lett. 2013;587:3824-30.
[52] Polizzi SJ, Walsh RM, Jr., Peeples WB, Lim JM, Wells L, Wood ZA. Human UDP-alpha-D-xylose synthase and *Escherichia coli* ArnA conserve a conformational shunt that controls whether xylose or 4-keto-xylose is produced. Biochemistry. 2012;51:8844-55.
[53] Merkx-Jacques A, Obhi RK, Bethune G, Creuzenet C. The *Helicobacter pylori* flaA1 and wbpB genes control lipopolysaccharide and flagellum synthesis and function. J Bacteriol. 2004;186:2253-65.
[54] Schirm M, Soo EC, Aubry AJ, Austin J, Thibault P, Logan SM. Structural, genetic and functional characterization of the flagellin glycosylation process in *Helicobacter pylori*. Mol Microbiol. 2003;48:1579-92.
[55] Studier FW. Use of bacteriophage T7 lysozyme to improve an inducible T7 expression system. J Mol Biol. 1991;219:37-44.
[56] Chang AC, Cohen SN. Construction and characterization of amplifiable multicopy DNA cloning vehicles derived from the P15A cryptic miniplasmid. J Bacteriol. 1978;134:1141-56.
[57] Sambrook J, Russell DW. Molecular cloning : a laboratory manual. 3rd ed. Cold Spring Harbor, N.Y.: Cold Spring Harbor Laboratory Press; 2001.

[58] Bertani G. Lysogeny at mid-twentieth century: P1, P2, and other experimental systems. J Bacteriol. 2004;186:595-600.
[59] Studier FW. Protein production by auto-induction in high density shaking cultures. Protein Expr Purif. 2005;41:207-34.
[60] Kibbe WA. OligoCalc: an online oligonucleotide properties calculator. Nucleic Acids Res. 2007;35:W43-6.
[61] Untergasser A, Cutcutache I, Koressaar T, Ye J, Faircloth BC, Remm M, et al. Primer3--new capabilities and interfaces. Nucleic Acids Res. 2012;40:e115.
[62] Snyder LR, Kirkland JJ, Dolan JW. Introduction to modern liquid chromatography. 3rd ed. Hoboken, N.J.: Wiley; 2010.
[63] Niesen FH, Berglund H, Vedadi M. The use of differential scanning fluorimetry to detect ligand interactions that promote protein stability. Nat Protoc. 2007;2:2212-21.
[64] Simeonov A. Recent developments in the use of differential scanning fluorometry in protein and small molecule discovery and characterization. Expert Opin Drug Discov. 2013;8:1071-82.
[65] Senisterra GA, Finerty PJ, Jr. High throughput methods of assessing protein stability and aggregation. Mol Biosyst. 2009;5:217-23.
[66] Ghai R, Falconer RJ, Collins BM. Applications of isothermal titration calorimetry in pure and applied research--survey of the literature from 2010. J Mol Recognit. 2012;25:32-52.
[67] Ladbury JE. Calorimetry as a tool for understanding biomolecular interactions and an aid to drug design. Biochem Soc Trans. 2010;38:888-93.
[68] Liang Y. Applications of isothermal titration calorimetry in protein science. Acta Biochim Biophys Sin (Shanghai). 2008;40:565-76.
[69] Perozzo R, Folkers G, Scapozza L. Thermodynamics of protein-ligand interactions: history, presence, and future aspects. J Recept Signal Transduct Res. 2004;24:1-52.
[70] Rhodes G. Crystallography made crystal clear : a guide for users of macromolecular models. 3rd ed. Amsterdam ; Boston: Elsevier/Academic Press; 2006.
[71] Rupp B. Biomolecular Crystallography : Principles, Practice, and Application to Structural Biology. New York: Garland Science; 2010.
[72] Wlodawer A, Minor W, Dauter Z, Jaskolski M. Protein crystallography for aspiring crystallographers or how to avoid pitfalls and traps in macromolecular structure determination. FEBS J. 2013;280:5705-36.
[73] Wooh JW, Kidd RD, Martin JL, Kobe B. Comparison of three commercial sparse-matrix crystallization screens. Acta Crystallogr D Biol Crystallogr. 2003;59:769-72.
[74] Garman E. 'Cool' crystals: macromolecular cryocrystallography and radiation damage. Curr Opin Struct Biol. 2003;13:545-51.
[75] O'Neill P, Stevens DL, Garman EF. Physical and chemical considerations of damage induced in protein crystals by synchrotron radiation: a radiation chemical perspective. J Synchrotron Radiat. 2002;9:329-32.
[76] Dauter Z. Data-collection strategies. Acta Crystallogr D Biol Crystallogr. 1999;55:1703-17.
[77] Kavanagh KL, Jornvall H, Persson B, Oppermann U. Medium- and short-chain dehydrogenase/reductase gene and protein families : the SDR superfamily: functional and structural diversity within a family of metabolic and regulatory enzymes. Cell Mol Life Sci. 2008;65:3895-906.
[78] Thoden JB, Frey PA, Holden HM. Molecular structure of the NADH/UDP-glucose abortive complex of UDP-galactose 4-epimerase from *Escherichia coli*: implications for the catalytic mechanism. Biochemistry. 1996;35:5137-44.
[79] Creuzenet C, Urbanic RV, Lam JS. Structure-function studies of two novel UDP-GlcNAc C6 dehydratases/C4 reductases. Variation from the SYK dogma. J Biol Chem. 2002;277:26769-78.

[80] Leclerc G, Wang SP, Ely B. A new class of *Caulobacter crescentus* flagellar genes. J Bacteriol. 1998;180:5010-9.
[81] Szymanski CM, Yao R, Ewing CP, Trust TJ, Guerry P. Evidence for a system of general protein glycosylation in *Campylobacter jejuni*. Mol Microbiol. 1999;32:1022-30.
[82] Sharma SK, Goloubinoff P, Christen P. Heavy metal ions are potent inhibitors of protein folding. Biochem Biophys Res Commun. 2008;372:341-5.
[83] Liu Y, Vanhooke JL, Frey PA. UDP-galactose 4-epimerase: NAD+ content and a charge-transfer band associated with the substrate-induced conformational transition. Biochemistry. 1996;35:7615-20.
[84] Thoden JB, Wohlers TM, Fridovich-Keil JL, Holden HM. Human UDP-galactose 4-epimerase. Accommodation of UDP-N-acetylglucosamine within the active site. J Biol Chem. 2001;276:15131-6.
[85] Schulz JM, Watson AL, Sanders R, Ross KL, Thoden JB, Holden HM, et al. Determinants of function and substrate specificity in human UDP-galactose 4'-epimerase. J Biol Chem. 2004;279:32796-803.
[86] D'Arcy A, Chaillet M, Schiering N, Villard F, Lim SP, Lefeuvre P, et al. Purification and crystallization of dengue and West Nile virus NS2B-NS3 complexes. Acta Crystallogr Sect F Struct Biol Cryst Commun. 2006;62:157-62.
[87] Snyder L, Snyder L. Molecular genetics of bacteria. 4th ed. Washington, DC: ASM Press; 2013.
[88] Datsenko KA, Wanner BL. One-step inactivation of chromosomal genes in *Escherichia coli* K-12 using PCR products. Proc Natl Acad Sci U S A. 2000;97:6640-5.
[89] Ishikawa M, Hori K. A new simple method for introducing an unmarked mutation into a large gene of non-competent Gram-negative bacteria by FLP/FRT recombination. BMC Microbiol. 2013;13:86.
[90] Hoang TT, Karkhoff-Schweizer RR, Kutchma AJ, Schweizer HP. A broad-host-range Flp-FRT recombination system for site-specific excision of chromosomally-located DNA sequences: application for isolation of unmarked *Pseudomonas aeruginosa* mutants. Gene. 1998;212:77-86.
[91] Kaniga K, Delor I, Cornelis GR. A wide-host-range suicide vector for improving reverse genetics in Gram-negative bacteria: inactivation of the blaA gene of *Yersinia enterocolitica*. Gene. 1991;109:137-41.
[92] Ried JL, Collmer A. An nptI-sacB-sacR cartridge for constructing directed, unmarked mutations in Gram-negative bacteria by marker exchange-eviction mutagenesis. Gene. 1987;57:239-46.
[93] Schweizer HP. Allelic exchange in *Pseudomonas aeruginosa* using novel ColE1-type vectors and a family of cassettes containing a portable oriT and the counter-selectable *Bacillus subtilis* sacB marker. Mol Microbiol. 1992;6:1195-204.
[94] Joung JK, Ramm EI, Pabo CO. A bacterial two-hybrid selection system for studying protein-DNA and protein-protein interactions. Proc Natl Acad Sci U S A. 2000;97:7382-7.
[95] Kallberg Y, Oppermann U, Jornvall H, Persson B. Short-chain dehydrogenases/reductases (SDRs). Eur J Biochem. 2002;269:4409-17.
[96] Feng HT, Wong N, Wee S, Lee MM. Simultaneous determination of 19 intracellular nucleotides and nucleotide sugars in Chinese Hamster ovary cells by capillary electrophoresis. J Chromatogr B Analyt Technol Biomed Life Sci. 2008;870:131-4.
[97] Nieba L, Nieba-Axmann SE, Persson A, Hamalainen M, Edebratt F, Hansson A, et al. BIACORE analysis of histidine-tagged proteins using a chelating NTA sensor chip. Anal Biochem. 1997;252:217-28.
[98] Gershon PD, Khilko S. Stable chelating linkage for reversible immobilization of oligohistidine tagged proteins in the BIAcore surface plasmon resonance detector. J Immunol Methods. 1995;183:65-76.

[99] Stefanowicz A. The biolog plates technique as a tool in ecological studies of microbial communities. Polish Journal of Environmental Studies. 2006;15:669-76.
[100] Garland JL, Mills AL. Classification and characterization of heterotrophic microbial communities on the basis of patterns of community-level sole-carbon-source utilization. Appl Environ Microbiol. 1991;57:2351-9.
[101] Baudoin E, Benizri E, Guckert A. Metabolic fingerprint of microbial communities from distinct maize rhizosphere compartments. European Journal of Soil Biology. 2001;37:85-93.
[102] Zhang H, Aebersold R. Isolation of glycoproteins and identification of their N-linked glycosylation sites. Methods Mol Biol. 2006;328:177-85.
[103] Kovacs JK, Felso P, Emody L, Schneider G, Kocsis B. Improved isolation protocol to detect high molecular weight polysaccharide structures of *Campylobacter jejuni*. J Microbiol Methods. 2014;107C:55-7.